

REPORT DOCUMENTATION PAGE

AD-A203 729

DTIC  
SELECTED

11. RESTRICTIVE MARKINGS

DTIC FILE COPY

12. DISTRIBUTION/AVAILABILITY OF REPORT

Approved for Public Release  
Distribution Unlimited

13. DATE OF PUBLICATION/DOWNGRADING REPORT NUMBER

1989

14. PERFORMING ORGANIZATION REPORT NUMBER

D 85

15. MONITORING ORGANIZATION REPORT NUMBER

AFOSR-TR- 89-0058

16a. NAME OF PERFORMING ORGANIZATION  
Northwestern University  
Department of Civil Engineering

16b. OFFICE SYMBOL  
(If applicable)

17a. NAME OF MONITORING ORGANIZATION

AFOSR/NA

16c. ADDRESS (City, State and ZIP Code)

Evanston, Illinois 60201

17b. ADDRESS (City, State, and ZIP Code)

Air Force Office of Scientific Research  
AFOSR/NA  
Bolling AFB, DC 20332

16d. NAME OF FUNDING/SPONSORING ORGANIZATION  
AIR FORCE  
Office of Scientific Research

16e. OFFICE SYMBOL  
(If applicable)  
AFOSR/NA

18. PROCUREMENT INSTRUMENT IDENTIFICATION NUMBER

AFOSR-85-0261

16f. ADDRESS (City, State and ZIP Code)

Bolling Air Force Base  
Washington, D. C. 20332

19. SOURCE OF FUNDING NOS

PROGRAM ELEMENT NO.	PROJECT NO.	TASK NO.	WORK UNIT NO.
61102F	2302	C2	

11. TITLE (Include Security Classification)  
"MICROSTRUCTURE AND CRACK INITIATION, PROPAGATION & LOCALIZATION IN CONCRETE"

12. PERSONAL AUTHOR(S)

Surendra P. Shah

13a. TYPE OF REPORT

Final

13b. TIME COVERED

FROM 6/85 TO 6/88

14. DATE OF REPORT (Yr., Mo., Day)

September 30, 1988

15. PAGE COUNT

50

16. SUPPLEMENTARY NOTATION

17. COSATI CODES

FIELD	GROUP	SUB. GR.

18. SUBJECT TERMS (Continue on reverse if necessary and identify by block number)

Acoustic Emission; Concrete fractures; Experiments; Laser Holographic Interferometry; Speckle Photography

19. ABSTRACT (Continue on reverse if necessary and identify by block number)

The goal of this research was to study the physical processes such as crack formation and localization affecting the performance of concrete. To clearly establish relation between macroscopic deformations and microscopic damage mechanisms, "model" concrete specimens with prefabricated microstructures were stressed and examined using Acoustic Emission and Laser Holography. The emphasis of the study was on a detailed observation of microstructure and crack growth under well defined boundary conditions. Fracture mechanics concepts were applied to understand various experimentally observed phenomena for different modes. *Keywords: crack propagation;*

(KT)

20. DISTRIBUTION/AVAILABILITY OF ABSTRACT

UNCLASSIFIED/UNLIMITED  SAME AS RPT.  DTIC USERS

21. ABSTRACT SECURITY CLASSIFICATION

UNCLASSIFIED

22a. NAME OF RESPONSIBLE INDIVIDUAL

Dr. Spencer Wu

22b. TELEPHONE NUMBER (Include Area Code)

(202)767-4935

22c. OFFICE SYMBOL

AFOSR/NA

AFOSR-TR- 89-0058

Approved for public release;  
distribution unlimited.

FINAL REPORT

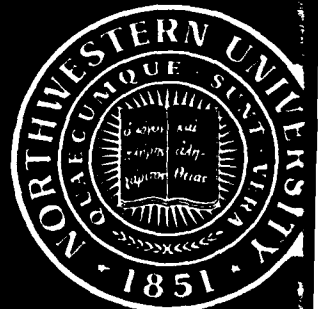
MICROSTRUCTURE AND CRACK INITIATION,  
PROPAGATION AND LOCALIZATION IN CONCRETE

AFOSR - 85 - 0261

PRINCIPAL INVESTIGATOR: S. P. SHAH

AIR FORCE OFFICE OF SCIENTIFIC RESEARCH (AFOSR)  
NOTICE: This report is available to DTIC  
The report has been reviewed and is  
approved for public release (AW AFR 190-12).  
Distribution is unlimited.  
MATTHEW J. KERPER  
Chief, Technical Information Division

**Technological Institute**  
**NORTHWESTERN UNIVERSITY**  
EVANSTON, ILLINOIS



FINAL REPORT  
MICROSTRUCTURE AND CRACK INITIATION,  
PROPAGATION AND LOCALIZATION IN CONCRETE

AFOSR - 85 - 0261

PRINCIPAL INVESTIGATOR: S. P. SHAH



Accession For	
NTIS CRA&I	<input checked="" type="checkbox"/>
DTIC TAB	<input type="checkbox"/>
Unannounced	<input type="checkbox"/>
Justification _____	
By _____	
Distribution /	
Availability Codes	
Dist	Avail and/or Special
A-1	

89

2

8

038

## TABLE OF CONTENTS

	<u>Page</u>
REPORT DOCUMENT PAGE	
TABLE OF CONTENTS	
EXECUTIVE SUMMARY	i
LIST OF PUBLICATIONS	iii
PART I: A STUDY OF FRACTURE PROCESS ZONE USING ACOUSTIC EMISSION MEASUREMENTS	 1
I.1 ACOUSTIC EMISSION TECHNIQUE	1
I.2 ACOUSTIC EMISSION MONITORING SYSTEM	3
I.3 TEST SPECIMEN	3
I.4 TEST PROCEDURE	4
I.5 SUMMARY OF RESULTS	4
PART II. CRACK PROFILES IN MODE I MEASURED BY HOLOGRAPHIC INTERFEROMETRY	 10
II.1 INTRODUCTION	10
II.2 HOLOGRAPHIC INTERFEROMETRY	11
II.3 SPECIMEN	12
II.4 HOLOGRAPHIC ARRANGEMENT	13
II.5 CRACK PROFILES	15
II.6 COMPARISON WITH LEFM	15
II.7 CONCLUSIONS	17
PART III. STUDY OF FRACTURE UNDER UNIAXIAL COMPRESSION USING OPTICAL MICROSCOPY	 30
III.1 MIX PROPORTIONS AND CURING	30
III.2 PETROGRAPHY	30
III.3 RESULTS	30
PART IV. CRACK PROPAGATION IN UNIAXIAL COMPRESSION: HOLOGRAPHIC INTERFEROMETRY	 35
IV.1 TEST SPECIMEN	35
IV.2 TESTING PROCEDURE	35
IV.3 SPECKLE PHOTOGRAPHY	36
IV.4 EXPERIMENTAL RESULTS	37
IV.5 SUMMARY OF RESULTS	38
REFERENCES	49

## EXECUTIVE SUMMARY

The accuracy of computer based numerical analysis of concrete structures is often limited particularly when large deformation and post-peak response are concerned. A clearer picture of the physical processes such as crack formation and localization would improve the performance of concrete. The goal of this research was to obtain a better understanding of fracture processes.

To clearly establish relation between macroscopic deformations and microscopic damage mechanisms, "model" concrete specimens with prefabricated microstructure were stressed and examined using Acoustic Emission and Laser Holography. The Acoustic Emission technique provided information on internal microcracking while Laser Holography was used to study surface crack development. The experiments yielded information on the position and nature microcracks. It was possible to observe and measure crack surface displacements with a resolution of less than half a micron with Holographic Interferometry.

The emphasis of the study was on a detailed observation of microstructure and crack growth under well defined boundary conditions. Fracture Mechanics concepts were applied to understand various experimentally observed phenomena for different modes of fracture. Numerical and theoretical investigations were done for better understanding and interpretation of experimental results and to determine relevant material properties.

The final report is divided into four parts. In the first, a description of fracture process zone for Mode I (tensile) crack propagation observed using acoustic emission source location technique is given. It was observed that the fracture process zone extended well behind the crack tip. This indicated that unbroken ligaments and interlocking may exist behind the crack tip.

Measurements of crack profile for a crack propagating in Mode I were obtained using laser holographic interferometry. This study is summarized in Part II. A comparison of observed crack profiles with those predicted from linear elastic fracture mechanics (finite element analysis with singular elements) revealed that as crack become longer it has a more pinched profile as compared to the predicted one. This indicated that cohesive crack models proposed by many researchers for numerical analysis may be appropriate for concrete. A closing pressure versus crack opening displacement relationship is proposed based on the experimental data.

To study how cracks initiate, propagate and localize under uniaxial compression, specimens subjected to various levels of strains were sectioned, sliced, dyed and polished and were examined using optical microscopy (described in Part III). Distributed microcracks were observed both in the ascending and the descending (strain softening) parts of the stress-strain curve. However, localized cracking in the direction of the loading was observed around the peak of the stress-strain curve.

A study of model concrete specimens subjected to uniaxial compression conducted with the aid of laser holography is summarized in Part IV. Holographic interferometry revealed that cracks initiate at the aggregate-matrix interface. Laser speckle photography showed that the interface cracks formed under mixed mode loading and eventually propagated in Mode I conditions.

How cracks propagate under mixed-mode loading (combined tensile and shear modes) was studied using off-centered-notched beam specimens. A two parameter, theoretical fracture model was proposed. The validity of this model was examined with the test data on shear failure of large reinforced concrete beams. For brevity, this mixed-mode study is not described in detail in this final report. The details of this study as well as other

investigations supported by this grant are given in the journal articles which are separately listed in the report.

#### LIST OF PUBLICATIONS

1. Maji, A. K., and Shah, S. P., "Process Zone and Acoustic Emission Measurement in Concrete," Experimental Mechanics, March 1988.
2. Shah, S. P., and Sankar, R., "Internal Cracking and Strain Softening Response of Concrete under Uniaxial Compression," ACI Materials Journal, Vol. 84, No. 3, May-June 1987.
3. Maji, A. K., and Shah, S. P., "Application of Acoustic Emission and Laser Holography to Study Microfracture in Concrete," Accepted for publication, American Concrete Institute, Special Publication, 1988.
4. Alvarado, M., Shah, S. P., and John, R., "Mode I Fracture in Concrete Using Center Cracked Plate Specimens," Accepted for publication, Engineering Mechanics, Journal, ASCE.
5. Miller, R. A., Shah, S. P., and Bjelkhagen, H. I., "Crack Profiles in Mortar Measured by Laser Holographic Interferometry," Accepted for publication in Experimental Mechanics, 1988.
6. Shah, S. P., "Fracture Toughness of Cement Based Materials," Materials and Structures, RILEM, V. 21, 1988.
7. Jenq, Y. S. and Shah, S. P., "Mixed Mode Fracture of Concrete," (in press), International Journal of Fracture.
8. Jenq, Y. S. and Shah, S. P., "Shear Resistance of Reinforced Concrete Beams," to be published, American Concrete Institute's Special Publication.
9. Shah, S. P., "Experimental Methods for Determining Fracture Process Zone and Fracture Parameters," to be published in Engineering Fracture Mechanics.
10. Maji, A. K. and Shah, S. P., "A Study of the Fracture Process Zone of Concrete Using Acoustic Emission," Proceedings of the SEM Spring Conference, New Orleans, LA, June 8-13, 1986.
11. Qin, Q., "A New Microcrack Factor to Measure Damage in Loaded Concrete Body Quantitatively," A thesis submitted in partial fulfillment of the requirements for the degree of Master of Science, Department of Civil Engineering, Northwestern University, August 1986.
12. Sankar, R., "Fracture of Strain-Softening Concrete in Uniaxial Compression," A thesis submitted in partial fulfillment of the requirements for the degree of Master of Science, Department of Civil Engineering, Northwestern University, June 1986.
13. Alvarado, M., "Fracture Mechanics Study of a Center Cracked Plate with a Point Load Applied at the Center of the Crack," A thesis submitted in

partial fulfillment of the requirements for the degree of Master of Science, Department of civil Engineering, Northwestern University, August 1987.

14. A. Maji and S. P. Shah, "Initiation and Propagation of Bond Cracks as Detected by Laser Holography and Acoustic Emission," Symposium Proceedings of the Materials Research Society, Vol. 64, 1988.
15. Shah, S. P., "Fracture Toughness of Concrete," to be published in Fracture of Concrete and Rock, Springer Verlag Publishers, 1989.
16. Maji, A., "Study of Concrete Using Acoustic Emission and Laser Holography," Ph.D. Thesis, Northwestern University, 1988.
17. Maji, A. and Shah, S. P., "Experimental Observations of Cracking and Damage," Proceedings, Workshop on Strain Localization and Size Effect, Cachan, Paris, France, 1988.
18. Shah, S. P., "A Model to Predict Fracture of Concrete Subjected to Varying Strain Rates," Proceedings, AFWAL Symposium on Dynamic Constitutive Failure (Ed. T. Nicholas), Wright Patterson AFB, May 1988.

Part I: A STUDY OF FRACTURE PROCESS ZONE USING ACOUSTIC EMISSION MEASUREMENT

I.1 Acoustic Emission Technique

Acoustic Emissions are caused by sudden release of strain energy resulting in a microseismic activity which propagates through the material that can be detected on the surface as small vibrations. These vibrations can be detected by placing piezoelectric transducers on the surface of the specimens which would convert the vibrations to electric signals. Acoustic Emission (AE) events can be caused by microcracking, intergranular friction, debonding and other phenomena. AE is also caused by phase transformation in crystalline materials. AE signals generated during loading have been analyzed in several ways:

1) The rate of occurrence of AE activity has been used to predict the extent of internal damage caused by external stress (Hamstad, (1)). Since the AE events are caused by irreversible energy dissipation which is frequently associated with damage, this method offers a direct study of damage accumulation. It may be possible to identify impending structural failure from monitoring of AE activity.

2) AE energy has been used to determine the critical energy release rate (Izsumi et. al., (2)). In addition, it could be possible to study the energy associated in different failure mechanisms such as interface debonding, fibre pullout, microcracking, etc. Such information would be pertinent to adopting specific material models for cement composites.

3) Frequency content, rise time, and amplitude of AE signals have been used to distinguish various damage mechanisms occurring at different loading stages (Tanigawa et. al., (3)). It has been suggested that the characteristics of the signal such as the rise time (time between first arrival and peak amplitude) and frequency content could be used to get additional information on fracture.

4) A series of transducers can be used to detect AE activities. Based on the time difference between detection of the event at different transducers, its source can be located. The velocity of seismic propagation is measured by ultrasonic techniques. The signals from the piezoelectric transducers is digitized and the time of first arrival of the signal is found from the digitized waveform. Progress of the FPZ has been studied using this technique (Labuz, Shah and Dowding, (4)).

5) Once the source is located, then by signal estimation of the AE waveform, the volume, orientation and type of cracking that caused the AE activity can be distinguished (Scruby et. al. (5), Michaels et. al. (6)).

The last two methods of analyzing AE signals can provide a powerful tool to examine the nature of fracture processes occurring in concrete and rock and are currently being employed at Northwestern University. In this research FPZ was studied by locating the source of AE events. The dimension of the specimens were such that a two dimensional analysis was conducted to locate the events; although it is possible to obtain a three dimensional

picture of FPZ using acoustic emissions (4). The two dimensional study was motivated due to the specimen thickness being only  $3/4$  " and because they were tested in uniaxial tension. In addition to locating the source of AE events, the rate of occurrence, frequency content and rise time of AE events at different loading stages were also studied.

### I.2 Acoustic Emission Monitoring System

The acoustic emission detection system was comprised of a) a four-channel digital oscilloscope (Nicolet 4094) with 2-MHz sampling rate, b) an IBM-AT personal computer, c) a general purpose interface bus (GPIB or IEEE 488), and d) signal analysis software.

Four piezoelectric transducers (Physical Acoustic Corp. PZT-5A) were used (Figure I.1). Each transducer was connected to a filter and a differential amplifier with a 60-dB gain between 200 kHz and 1.0 MHz. The amplified signal was digitized at 2 MHz and stored on the oscilloscope.

### I.3 Test Specimen

Two types of single-edge-notched specimens were tested in uniaxial tension: 1) mortar specimens, and 2) model-concrete specimens with prearranged inclusions. Model concrete specimens made with  $1/2$  " diameter limestone aggregates shown in Figure I.2 were used to study the effect of inclusions on a propagating crack.

The mortar used had a mix proportion by weight of 1:2:0.5 (cement:sand:water). ASTM Type I cement was used. The siliceous

sand used had a maximum size of 1/4" (6.35mm) (US sieve No. 4). Specimens were tested between 1 1/2 to 2 1/2 months from the day of casting. They were kept in a normal laboratory environment after the first 28 days.

#### I.4 Test Procedure

Tests were conducted in a 20-kip (89 kN) capacity closed-loop MTS testing machine. An extensometer mounted across the notch to measure the crack-mouth opening displacement (CMOD) was used as the feedback control. Cyclic loading and unloading was done on both mortar and concrete specimens. At frequent intervals, the displacement was held constant while the specimen surface was investigated for cracking by a 40 x microscope. The results of the cyclic loading test are shown in Figures I.3 and I.4 for plain mortar and model concrete specimens. The points at which the loading was stopped to optically (40x) observe the crack growth are lettered on the load-CMOD plots. Crack growth was observed on the surface of the specimen by a traveling microscope which was internally illuminated and was fitted with a micrometer. (See Reference 7 for details). This optically observed crack length is plotted in Figures I.3 and I.4 where the AE source locations are also plotted.

#### I.5 Summary of Results

1. AE events localize before peak load and the event location cluster progresses forward with increasing CMOD. Some events occur ahead of the crack tip but events continue to occur far behind the crack tip near the notch tip well into the strain

softening region. It is supposed that internal ligaments continue to carry load despite surface cracking (Fig. I.4).

2. Multiple peaks occur in model concrete specimens because of the crack being arrested and redirected by the aggregate (Fig. I.3). The peak load in model concrete specimens is attained at a much larger CMOD.

3. Rate of acoustic events increase sharply shortly before peak load. The highest rate occurs just after peak load is attained. For the two peak loads in model concrete specimens, two corresponding peaks are also observed in the event-rate vs. CMOD plot.

4. The occurrence of AE events behind the crack tip suggests that Dugdale-Barenblat type of cohesive crack model may be appropriate for predicting crack propagation in concrete. This is further described in the next section.

5. The effective crack length estimated from the modified LEFM model (two parameter fracture model developed by Jenq and Shah (9))

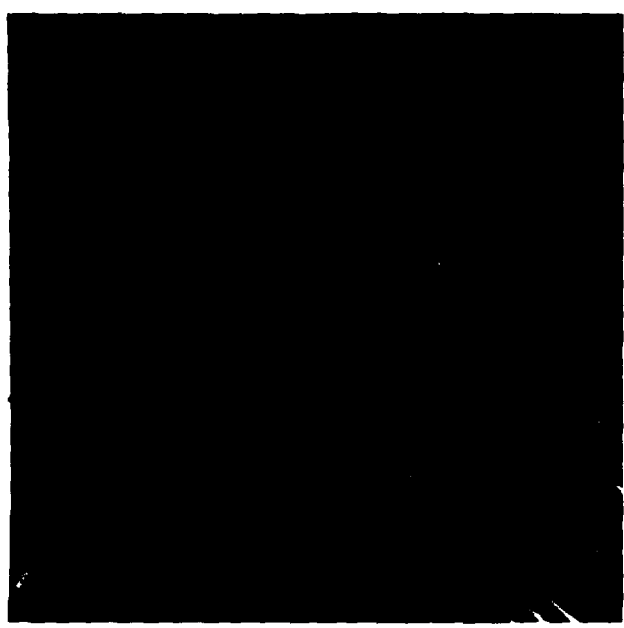
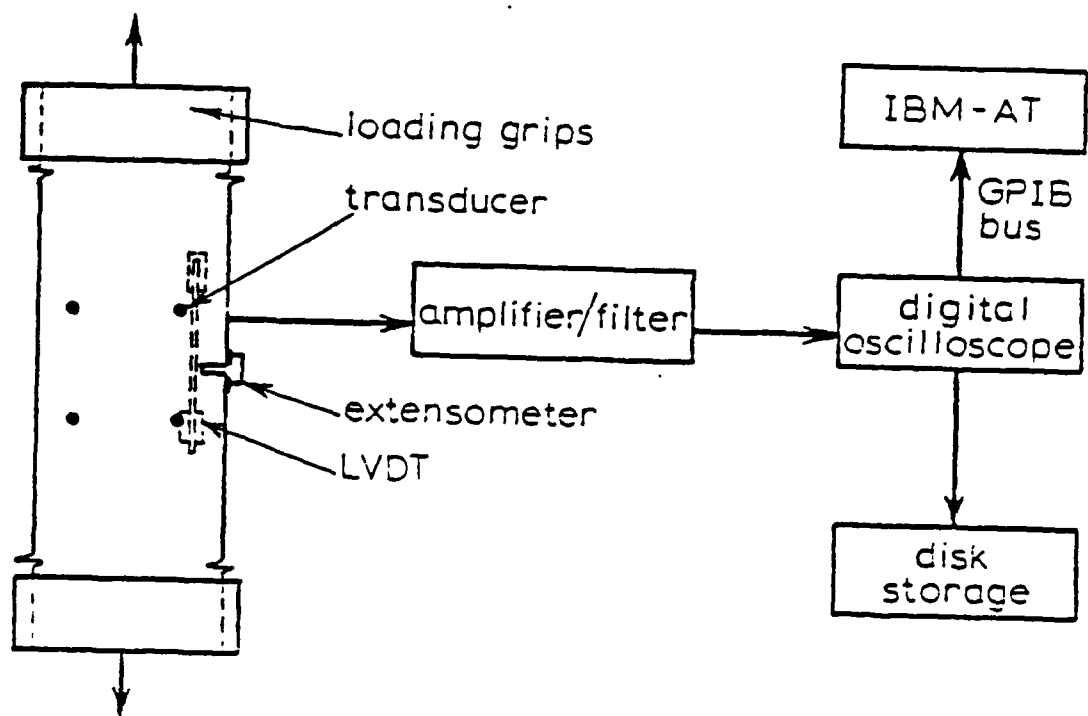


Figure I.1 SET-UP FOR ACOUSTIC EMISSION TESTS IN TENSION

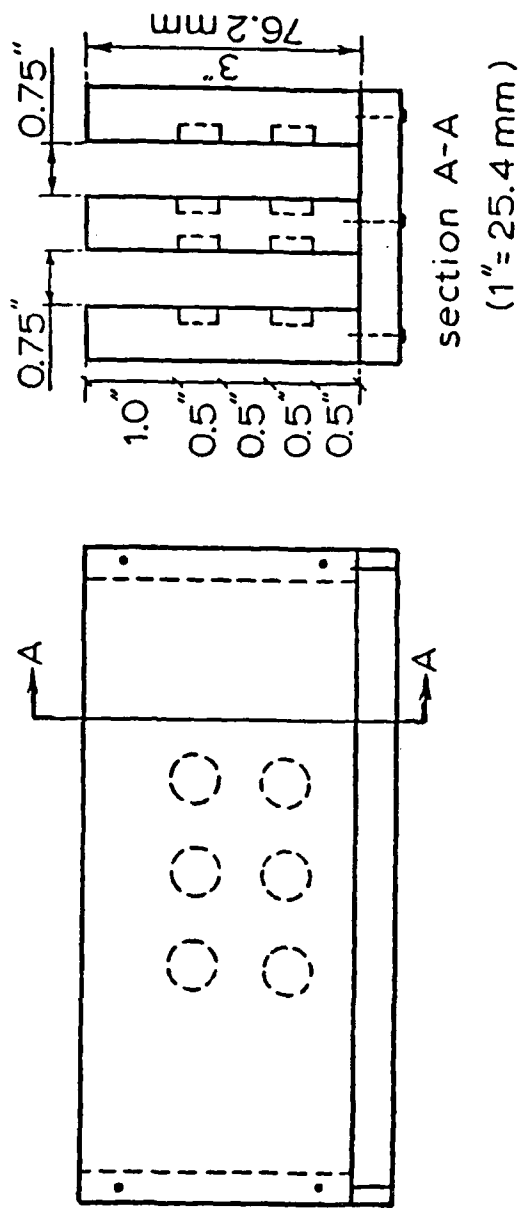


Figure I.2 MOLDS FOR CASTING MODEL CONCRETE SPECIMENS

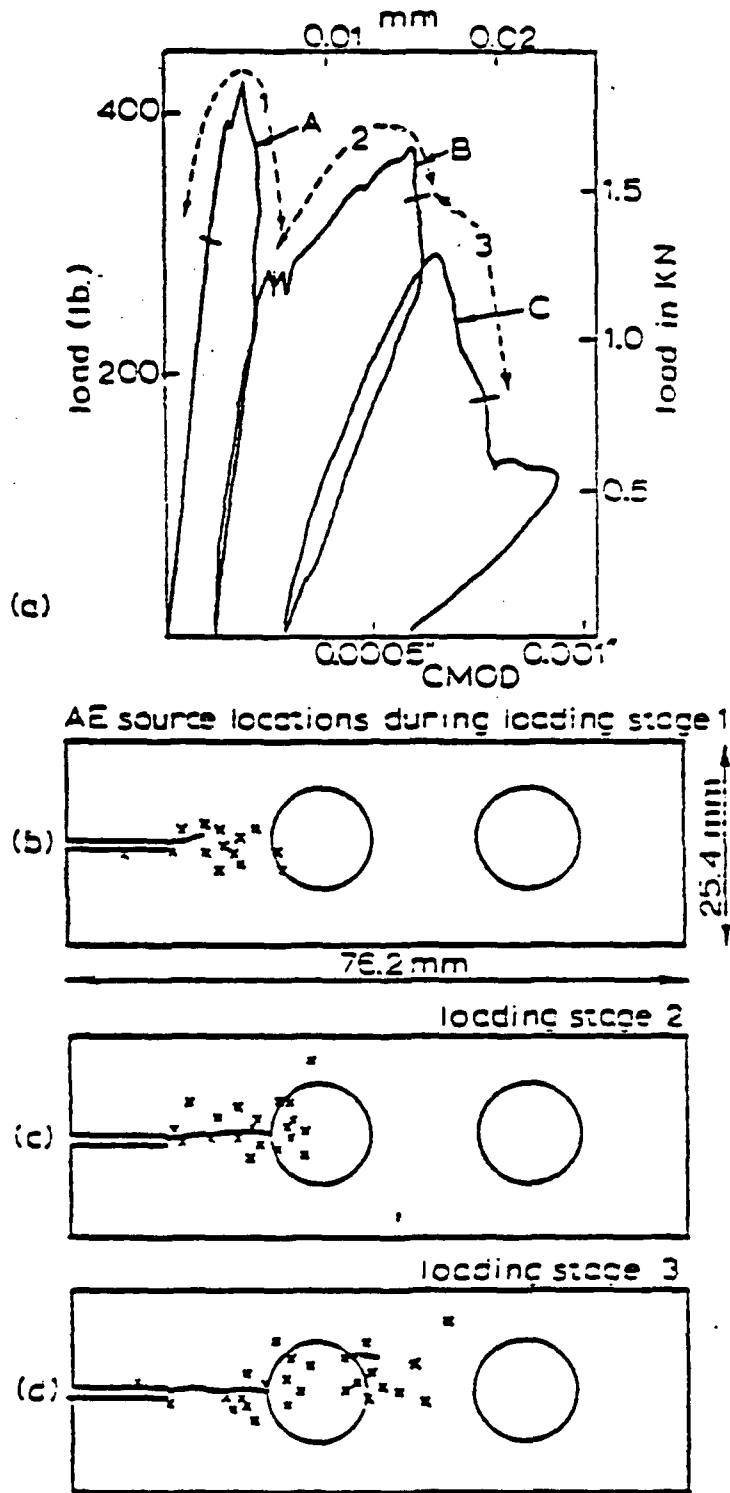
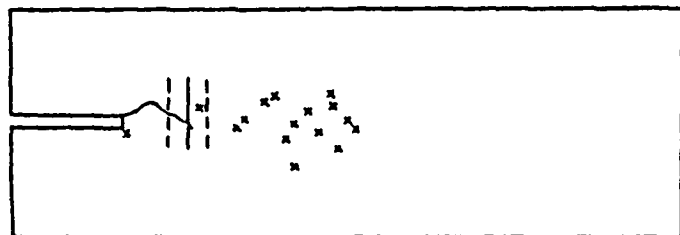
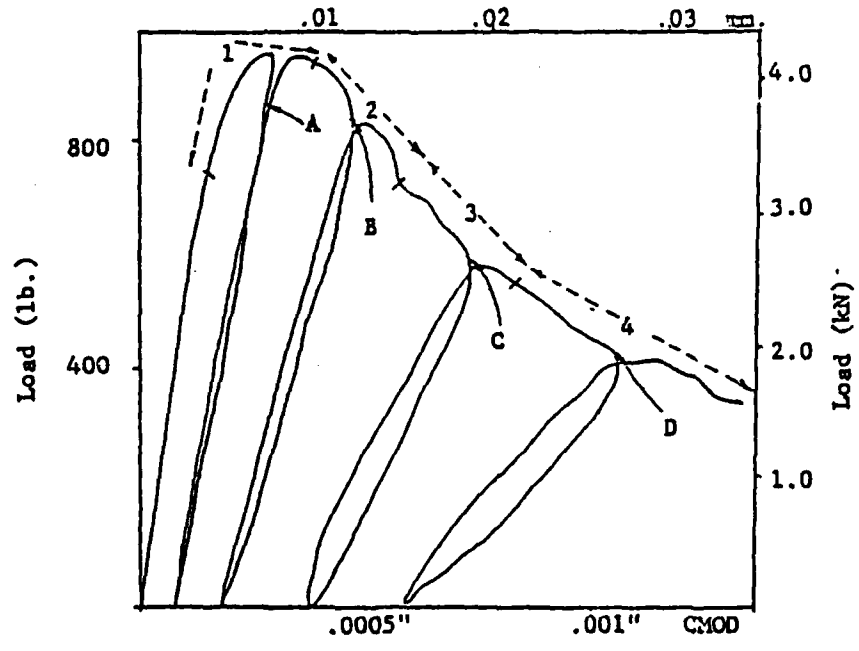
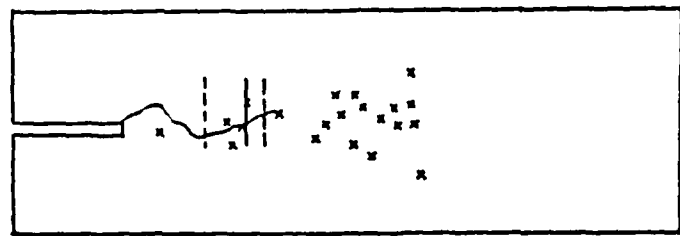


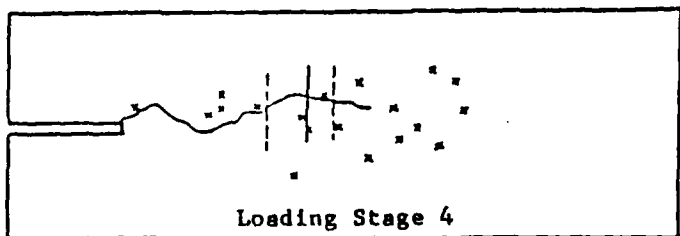
Figure I.3 AE SOURCE LOCATIONS FOR MODEL CONCRETE SPECIMEN



Loading Stage 2



Loading Stage 3



Loading Stage 4

Figure I.4 AE SOURCE LOCATIONS FOR PLAIN MORTAR SPECIMEN

## Part II: CRACK PROFILES IN MODE I MEASURED BY HOLOGRAPHIC INTERFEROMETRY

### II.1 Introduction

It is generally accepted that non-linear fracture models must be used to describe the cracking process in mortar. Several authors (8,9,10,11,12) have proposed models in which a closing pressure is applied to the crack. One way to test which of these models is appropriate is to compare the model predictions with measured crack opening profiles. Most researchers measure the crack opening displacement (COD) at one or two discrete points and make their comparisons with these few measurements. Until now, no one has been able to accurately measure the entire crack opening profile in concrete or mortar.

Laser holographic interferometry is ideally suited to measuring surface crack opening profiles. This method allows surface displacements to be measured across the entire object with an accuracy of less than  $1\mu\text{m}$ . Cracks are easily seen as discontinuities in the fringe pattern formed by the interferometry process. This allows cracks to be seen anywhere on the surface long before they are visible to the eye.

Previous attempts have been made to study cracking in concrete using laser holographic interferometry to observe crack patterns and to measure out-of-plane (perpendicular to the object surface) displacement. To the best of the authors' knowledge, no one has used holographic interferometry to obtain crack opening displacements in mode I cracks in concrete or mortar.

## II.2 Holographic Interferometry

A hologram is a complex diffraction grating which, when illuminated by a properly oriented beam of laser light, reproduces a three dimensional image of an object. The hologram is formed by recording the interference pattern of two light waves, the object wave and the reference wave. Object waves are formed by reflecting an expanded beam of laser light off an object onto a photographic material, while the reference wave is an expanded, but otherwise undisturbed, beam of laser light that is shone directly onto the photographic material. The two waves interfere and the interference pattern is recorded in the photographic emulsion. If the photographic material is developed, replaced in its original position, and then illuminated by the reference wave. the reference wave will be diffracted by the recorded interference patterns and reproduce an exact duplicate of the original object wave.

Since the reproduced object wave is made of laser light, it is possible to interfere with this wave. In holographic interferometry, two object waves, representing the object in two different states of deformation, are combined. The two waves then interfere with each other resulting in an image of the object covered with alternate light and dark fringes. These fringes quantitatively represent the movement, which occurred between the making of the two holograms, of each point on the object surface.

The type of interferogram used in this study is called a

sandwich hologram. Sandwich holograms are made by taking two separate holograms of the object in two different states of displacement and, after processing, gluing the holograms together. (The actual process is more complicated than this and has been omitted in the interest of brevity. Information on making sandwich holograms can be found in Abramson (13)). One of the problems with most types of interferograms is that they will record the effects of all displacement, including rigid body displacements. Fringe patterns created by rigid body motion can obscure the fringe patterns created by stress induced displacements, rendering the interferogram useless. The advantage to sandwich holography is that the effects of rigid body motion can be eliminated by rotating the sandwich hologram about a particular axis (13,14).

### II.3 Specimen

The specimen used in this study was a center cracked plate loaded by point loads at the midpoint of the crack (Figure II.1). The actual specimen used in this study was a mortar plate 12" x 12" x 1" (305mm x 305mm x 25mm). A 1" (25mm) loading hole with two diametrically opposed notches was cast into the center of the plate. The length of the notches, measured from the center of the loading hole, was 7/8" (22mm). The mortar used to cast the specimens had ratios of 1.00/2.60/0.65 (cement/sand/water) by weight. The specimens were tested in 20,000 pound (90 kN) capacity loading frame mounted on a vibration isolation table. Loading was accomplished by using the

"airplane" shaped pieces shown in Figures II.2 and II.3. The "nose" of the "airplane" is attached to a semi-cylindrical piece which applies the load to the specimen loading hole. Strain gaged steel bars connect the "wings" and, since they are loaded in parallel with the concrete, stabilize the growth of the crack in the concrete. The load in the concrete is determined by subtracting the load in the steel, as measured by the strain gages, from the total load read from a load cell.

#### II.4 Holographic Arrangement

The holograms used in this experiment were split beam transmission (Leith-Upatnieks type) holograms, as shown in Figure II.1 (note: the black box next to the plate holder in Figure II.2 is a monobath holographic film processor used to check the holographic system). A laser beam is split into two parts, one part illuminates the object and creates the object wave, while the other part of the beam creates the reference wave. A HeNe laser ( $\lambda=2.5 \times 10^{-5}$  in., 633nm) was used.

One important parameter in the holographic arrangement is the sensitivity vector,  $\vec{k}$ . The sensitivity vector is the bisector of the angle formed by the beam illuminating the object and the beam reflected from the object to the photographic plate. The fringe pattern seen in a holographic interferogram can be thought of as representing the projection of the surface displacement on the sensitivity vector. The displacement,  $\vec{d}$ , is found to be (1):

$$\vec{d} \cdot \vec{k} = \frac{n\lambda}{2\cos\alpha} \quad (1)$$

or, solving the dot product:

$$d = \frac{n\lambda}{2\cos\alpha\cos\sigma}$$

where:  $n$  = fringe order

$\lambda$  = wavelength of laser light

$\alpha$  = 1/2 angle between beam illuminating the object and beam reflected from object to the photographic plate

$\sigma$  = angle between  $\vec{d}$  and  $\vec{k}$

The fringes in the interferogram represent the projection of the displacement vector on the sensitivity vector. Since there is an infinite number of vectors with the same projection on the sensitivity vector, it is necessary to know the direction of the displacement before equation 1 can be used. However, in certain special cases it is possible to directly separate a desired component of motion without knowing the direction of the displacement beforehand. One such case allows in-plane displacement to be separated directly if the original displacement pattern is symmetric. This method was proposed by Nelson and McCrickerd (15).

The method described by Nelson and McCrickerd in their paper was not the most general case. The authors have solved the problem for the more general case. Consider two points on the surface of the object, A and A' (Figure II.3). From equation 1:

$$\vec{d}_{A'} \cdot \vec{k} = \frac{n_1\lambda}{2\cos\alpha} \quad (2a)$$

$$\vec{d}_A \cdot \vec{k} = \frac{n_2\lambda}{2\cos\sigma} \quad (2b)$$

subtracting yields:

$$(\vec{d}_{A'} - \vec{d}_A) \cdot \vec{k} = -\frac{n\lambda}{2\cos\alpha} \quad (2c)$$

in a specimen with symmetrical displacements where A and A' are symmetrical points,  $\vec{d}_{A'} - \vec{d}_A$  is the x direction component of displacement (Figure 3) and n is the number of fringes between points A and A'. The x displacement measured from the line of symmetry is given by:

$$x = \frac{n\lambda}{4\cos\alpha\cos\psi} \quad (3)$$

where:  $\psi$  = angle between  $\vec{k}$  and the x axis

### II.5 Crack Profiles

Figure II.4 shows a set of crack profiles from the in-plane sensitive holograms. It can be observed from the crack profiles shown in Figure II.4 that the crack tip opening displacements will sometimes increase over several load intervals before the crack propagates. Jenq and Shah (9,10) had suggested that there was a critical CTOD needed for crack propagation. Based on beam tests for the same type of mortar, Jenq and Shah had proposed a value of  $3.8 \times 10^{-4}$  inches ( $8.5 \mu\text{m}$ ) for the critical CTOD. This value corresponded well with the measurement obtained in this study.

### II.6 Comparison with LEFM

Holographically measured crack profiles were compared with those obtained using linear elastic fracture mechanics (LEFM). To obtain stress intensity factors and crack profiles for the

finite geometry of the specimens tested, finite element programs using quarter-point node singular elements were used (Fig. II.5).

A comparison of LEFM predicted crack profiles with those measured holographically is shown in figures II.6 and II.7. It can be seen that at low load and short crack lengths, there is little difference between the measured and the predicted crack profiles. However, for longer crack lengths, the holographically measured crack profiles are arrower than predicted LEFM crack profiles. This suggests the presence of a closing pressure in the crack.

To include the effect of fracture process zone in numerical analysis, many researchers use a Dugdale-Barenblat type of model (Milladay, Hawkins, Jenq and Shah). In this model, a closing pressure is applied on the crack surfaces. The amount of closing pressure is assumed to depend on crack opening displacement. Several relationships have been proposed to model the fracture process zone using this concept. In this study, closing pressure was determined so that the crack profile calculated using finite element analysis would match the experimentally measured crack profile.

A flexibility matrix was calculated for a unit load applied at each nodal point along the crack. The loads at the nodal points [P1, P2 ... Pn in Fig. II.8) were determined using simultaneous equations and flexibility matrix so that the calculated and the measured profile were the same. The calculated pressures for various crack lengths are shown in Figs.

II.10a and II.10b. Also shown are some of the suggested relationships between closing pressure and crack opening displacement. It was concluded that the relationship that best matched the experimental profiles was the bilinear relationship shown in Fig. II.11. In figure II.11, crack profile predicted using LEFM with the bilinear closing pressure as well as a crack profile for a Dugdale type model are shown. This profile was obtained using the bilinear closing pressure vs crack opening displacement relationship and assuming that the resultant stress intensity factor is zero. For many other loads, it was not often possible to find a crack length such that  $K_I = 0$ .

#### II.7 Conclusions

1. Holographic interferometry can be used to measure crack profiles in mortar to an accuracy of  $1.4 \times 10^{-5}$  inch ( $.4\mu\text{m}$ ).
2. Displacement of cracks in mortar appear to be concentrated at the crack tip.
3. There seems to be a limit as to how large the crack tip opening displacement can become before propagation of the crack. Although the data presented here shows considerable scatter, the value of critical crack tip opening displacement suggested by Jenq and Shah (16) of  $3.8 \times 10^{-4}$  inch ( $8.5 \mu\text{m}$ ) appears correct to an order of magnitude.
4. At low load levels and corresponding short crack lengths, there is little difference between measured crack profiles and profiles predicted by LEFM. The difference becomes greater under increasing load, suggesting that the influence of a fracture

process zone becomes greater with increasing load.

5. The holographically measured crack profiles are narrower than predicted LEFM crack profiles with the same crack length. This suggests the presence of a closing pressure on the crack.

6. A bilinear closing pressure vs. crack opening relationship produces a good correlation with experimental crack profiles.

7. The stress intensity factor for the crack with the bilinear closing pressure has a constant upper limit. This suggests that the critical stress intensity factor may be a valid fracture toughness parameter.

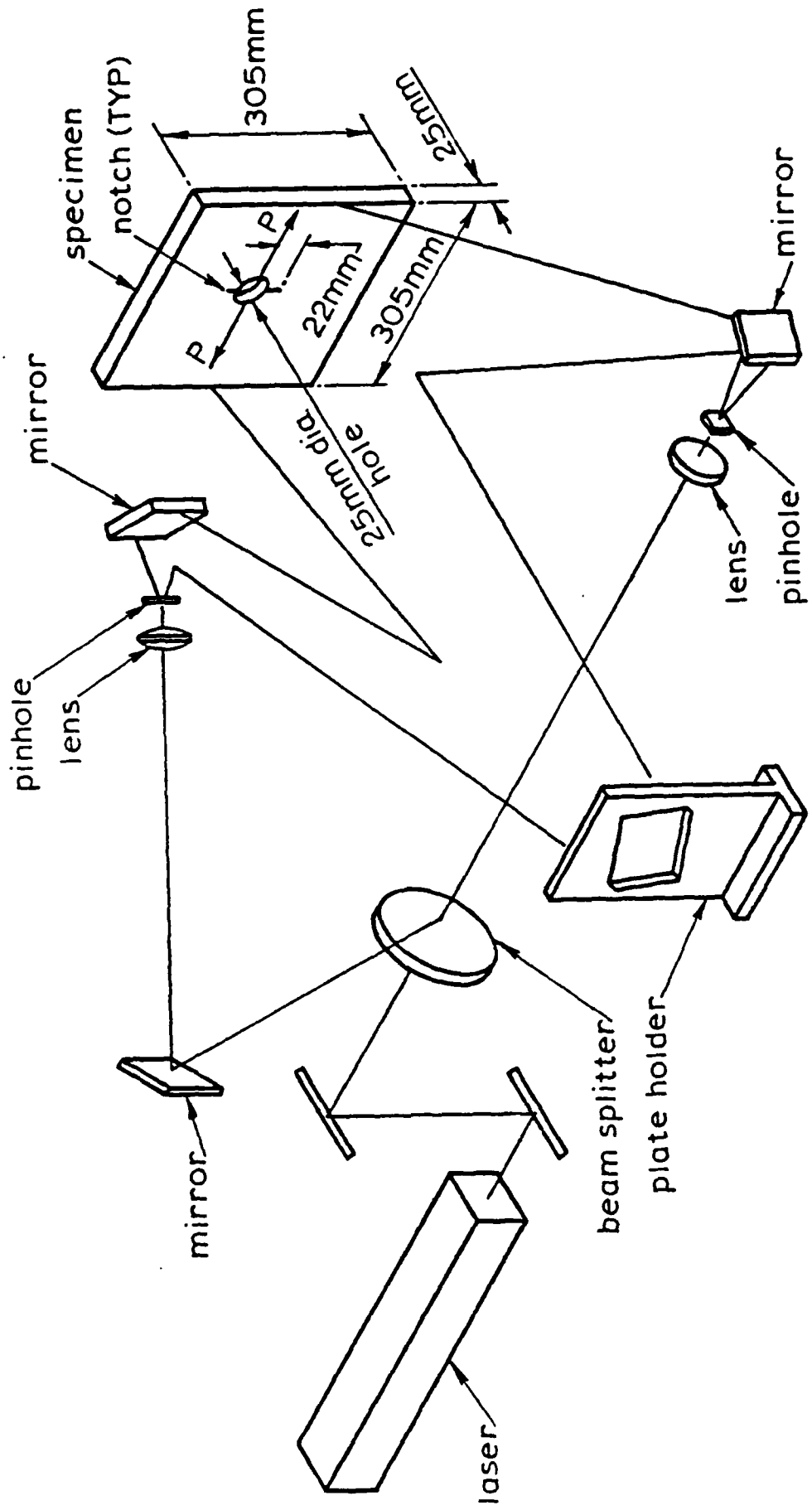


Figure II.1 HOLOGRAPHIC ARRANGEMENT AND SPECIMEN DIMENSIONS

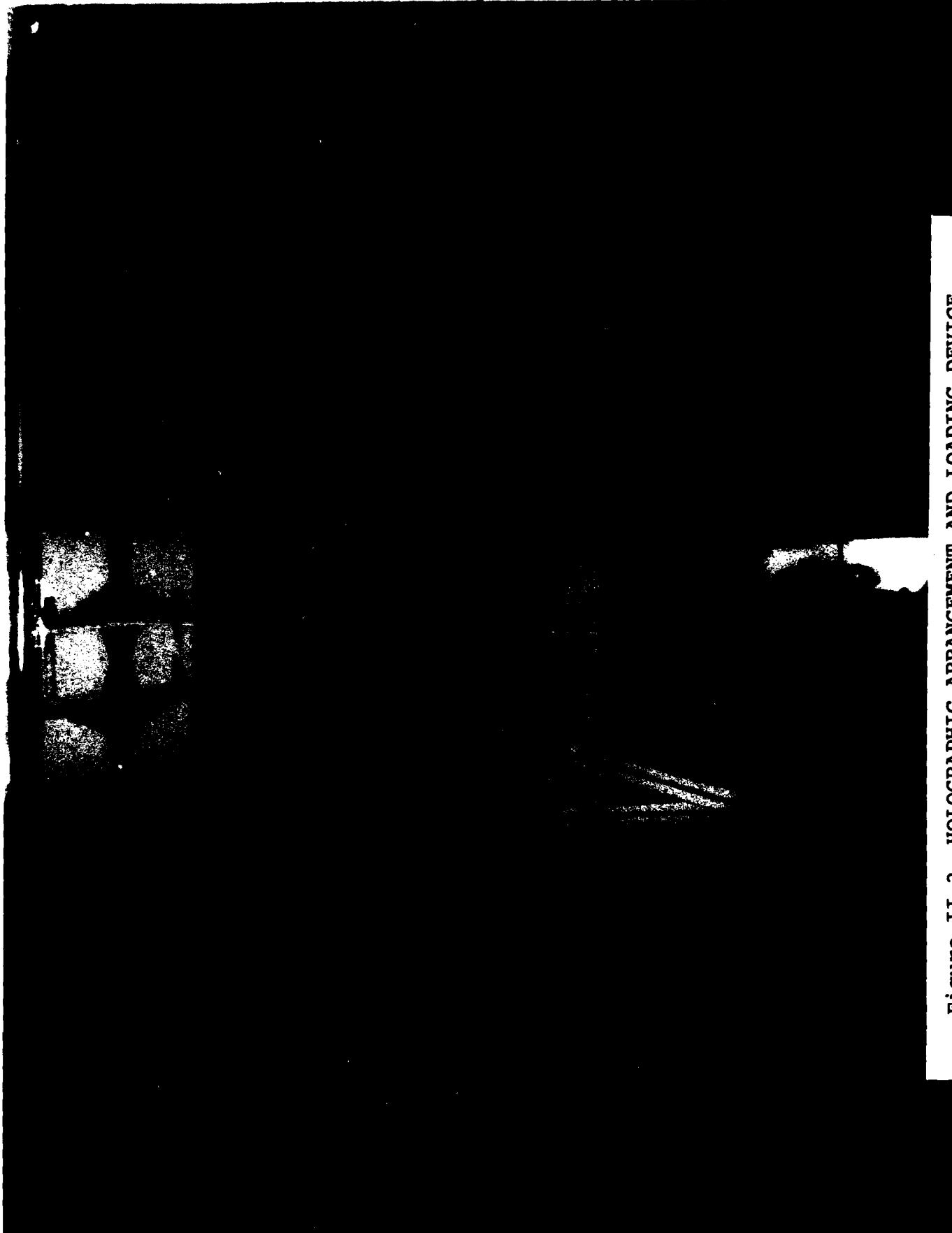


Figure II.2 HOLOGRAPHIC ARRANGEMENT AND LOADING DEVICE

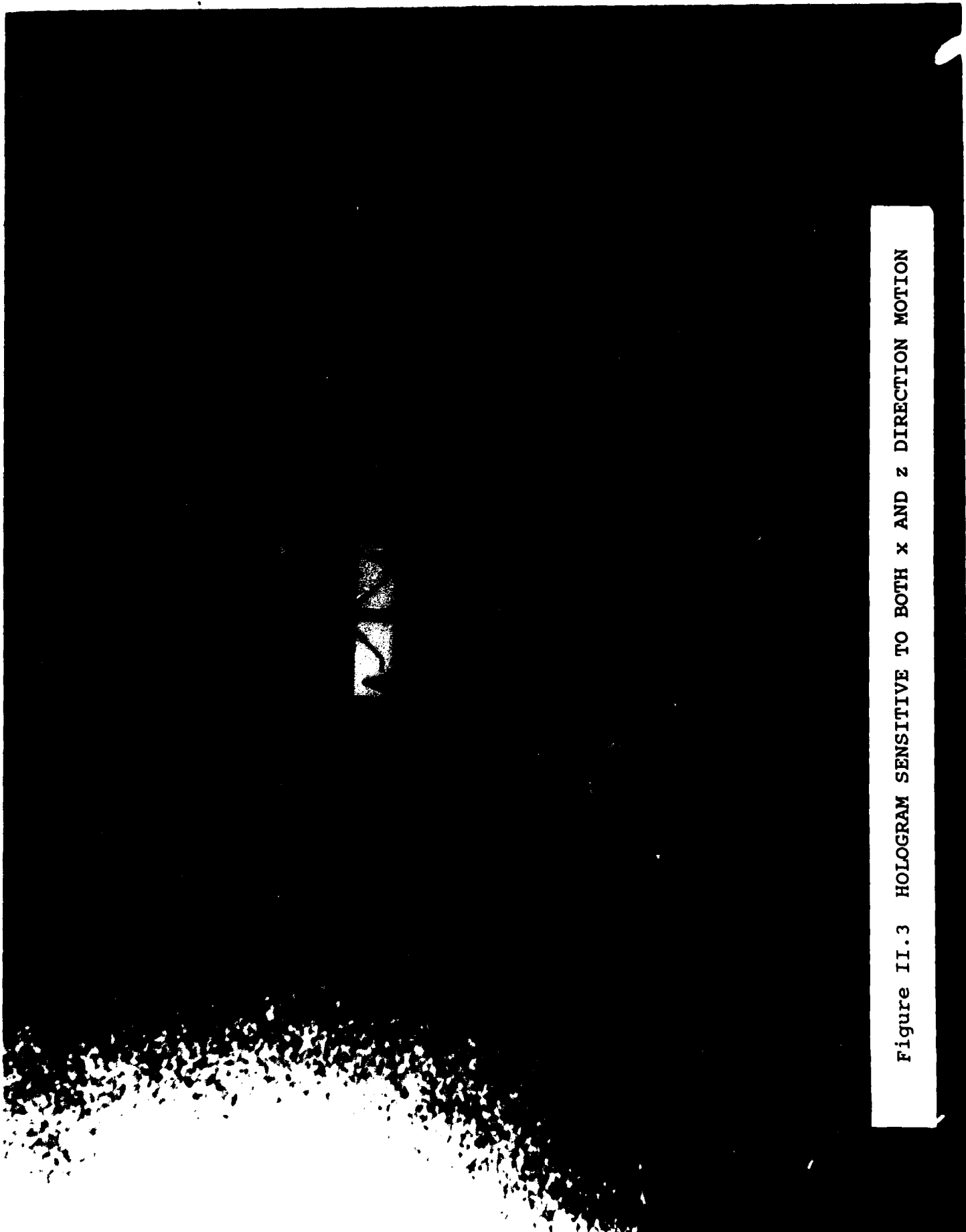


Figure II.3 HOLOGRAM SENSITIVE TO BOTH x AND z DIRECTION MOTION

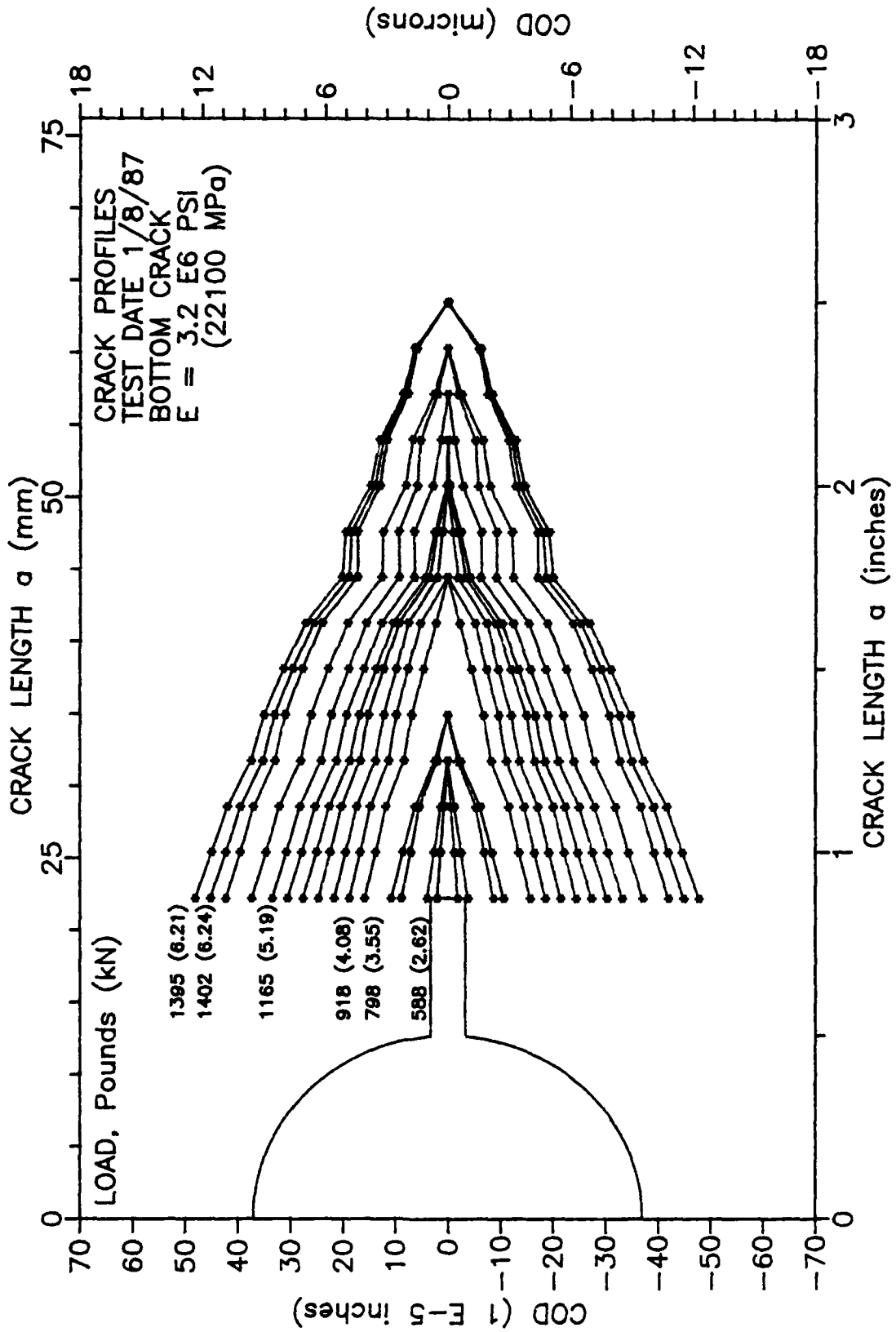


Figure II.4 HOLOGRAPHIC CRACK PROFILES FOR DIFFERENT CRACK LENGTHS

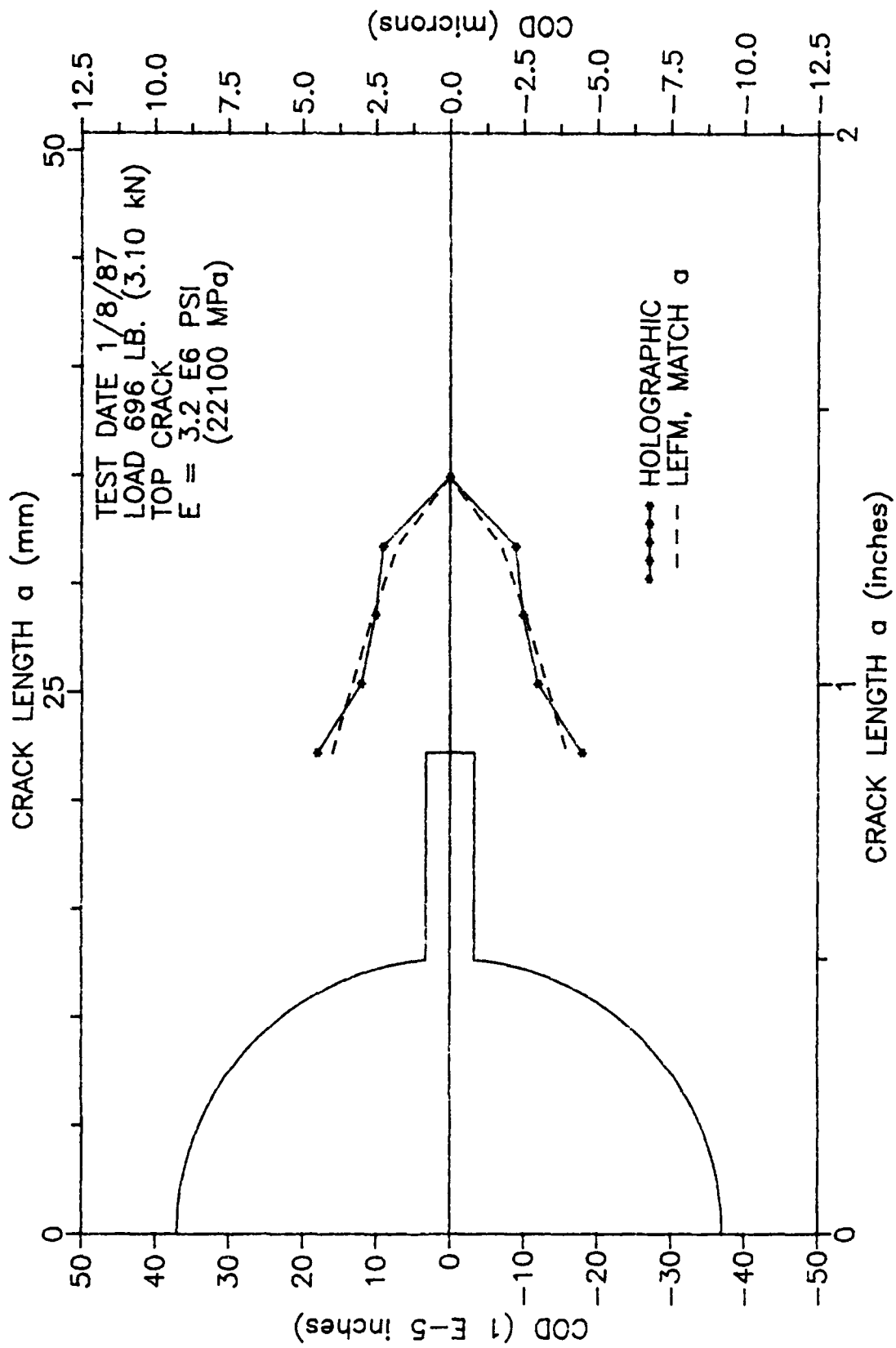


Figure II.5 HOLOGRAPHIC vs LEFM CRACK PROFILE COMPARISON. LOAD = 696 LB.

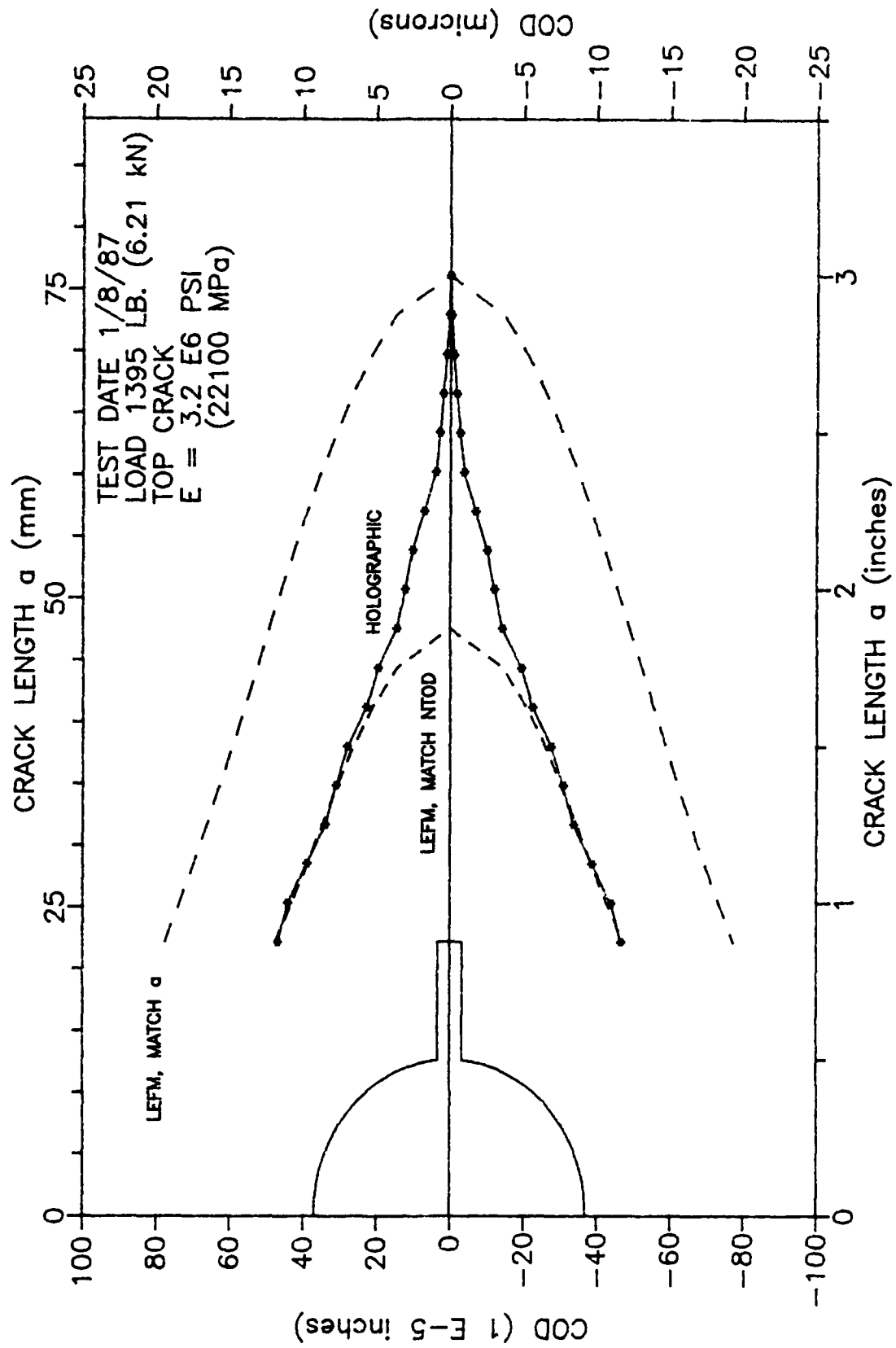


Figure II.6 HOLOGRAPHIC vs LEFM CRACK PROFILE COMPARISON. LOAD = 1395 LB.

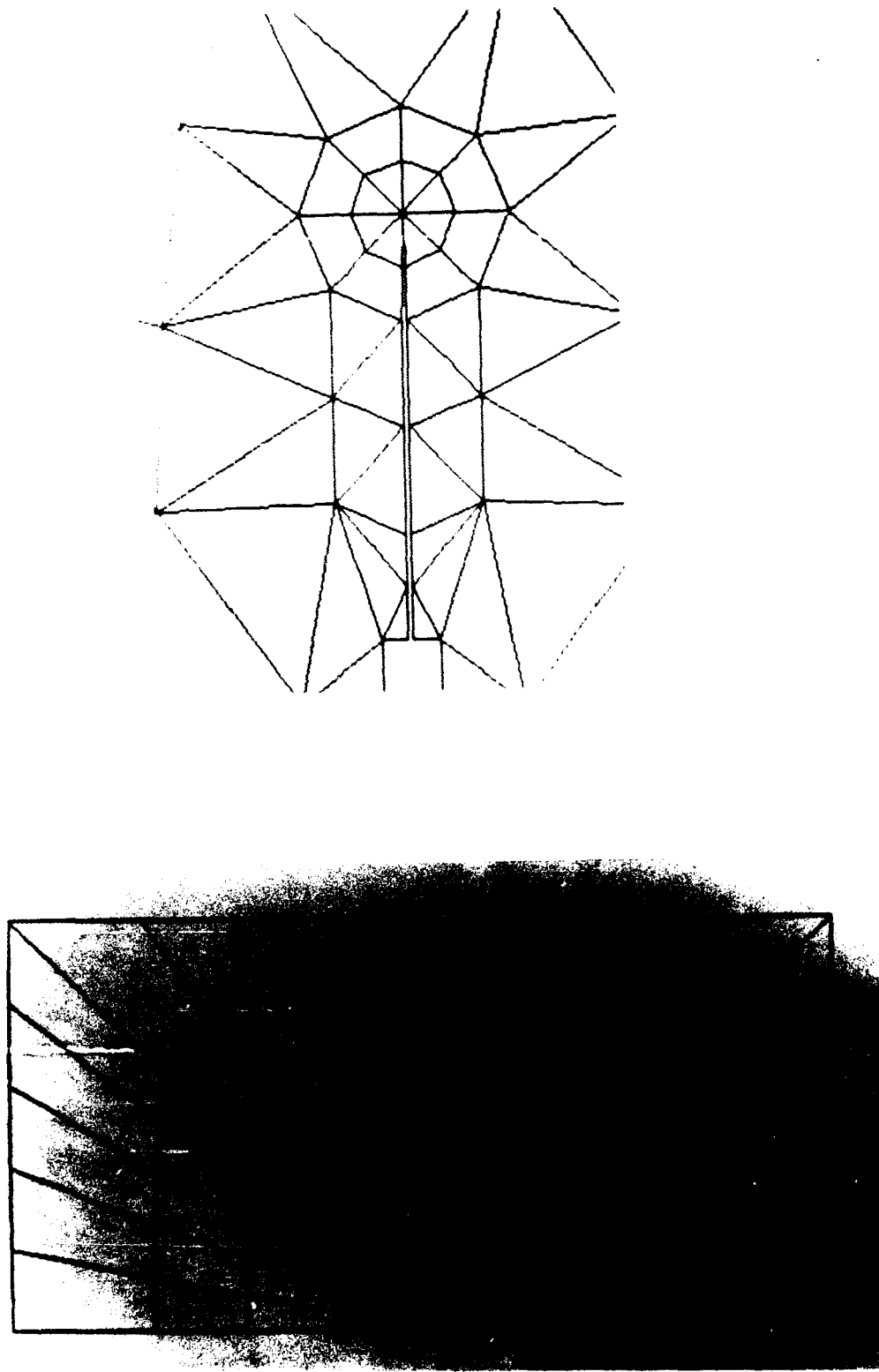


Figure II.7 FINITE ELEMENT MESH

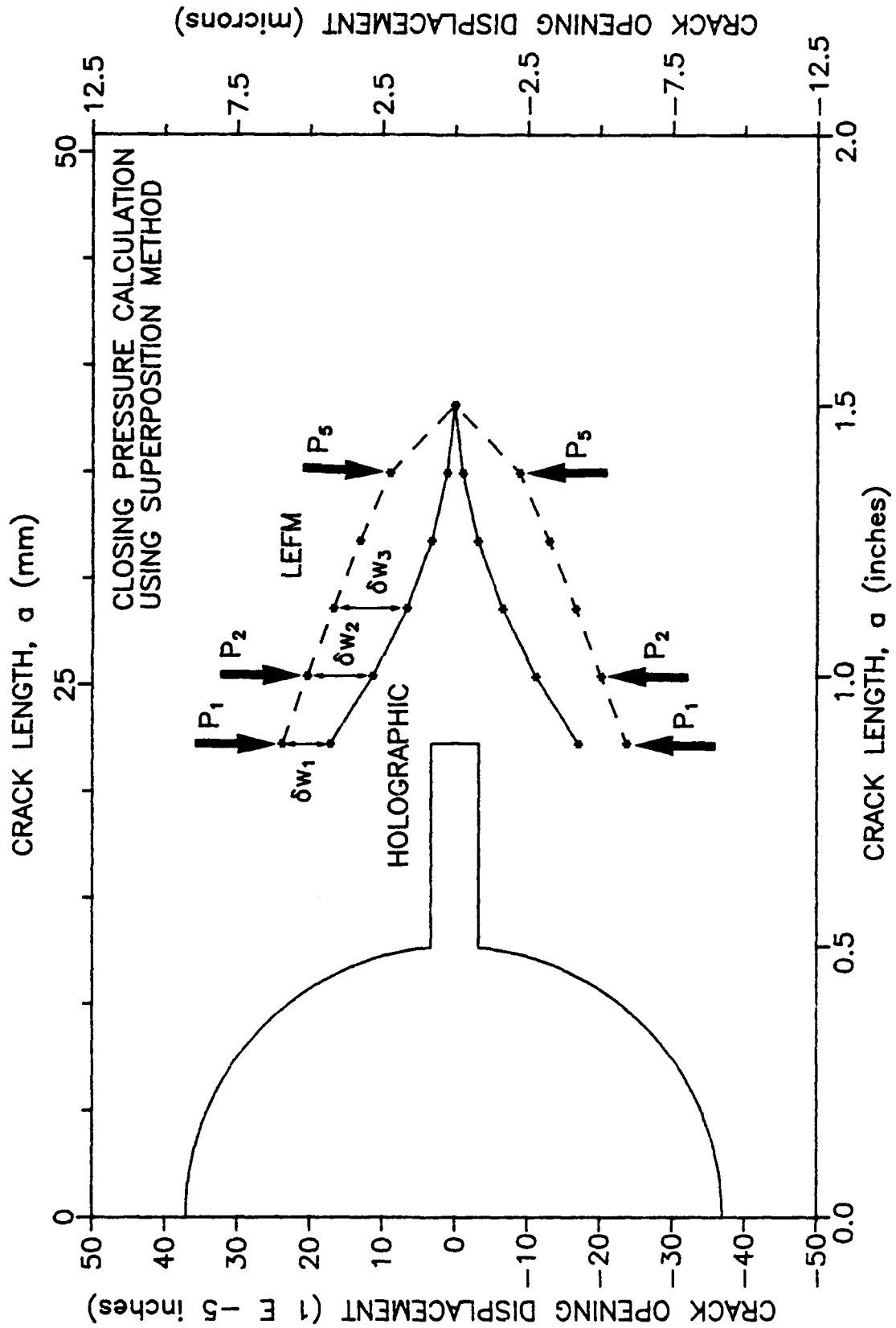


Figure II.8 CLOSING PRESSURE CALCULATION USING SUPERPOSITION METHOD

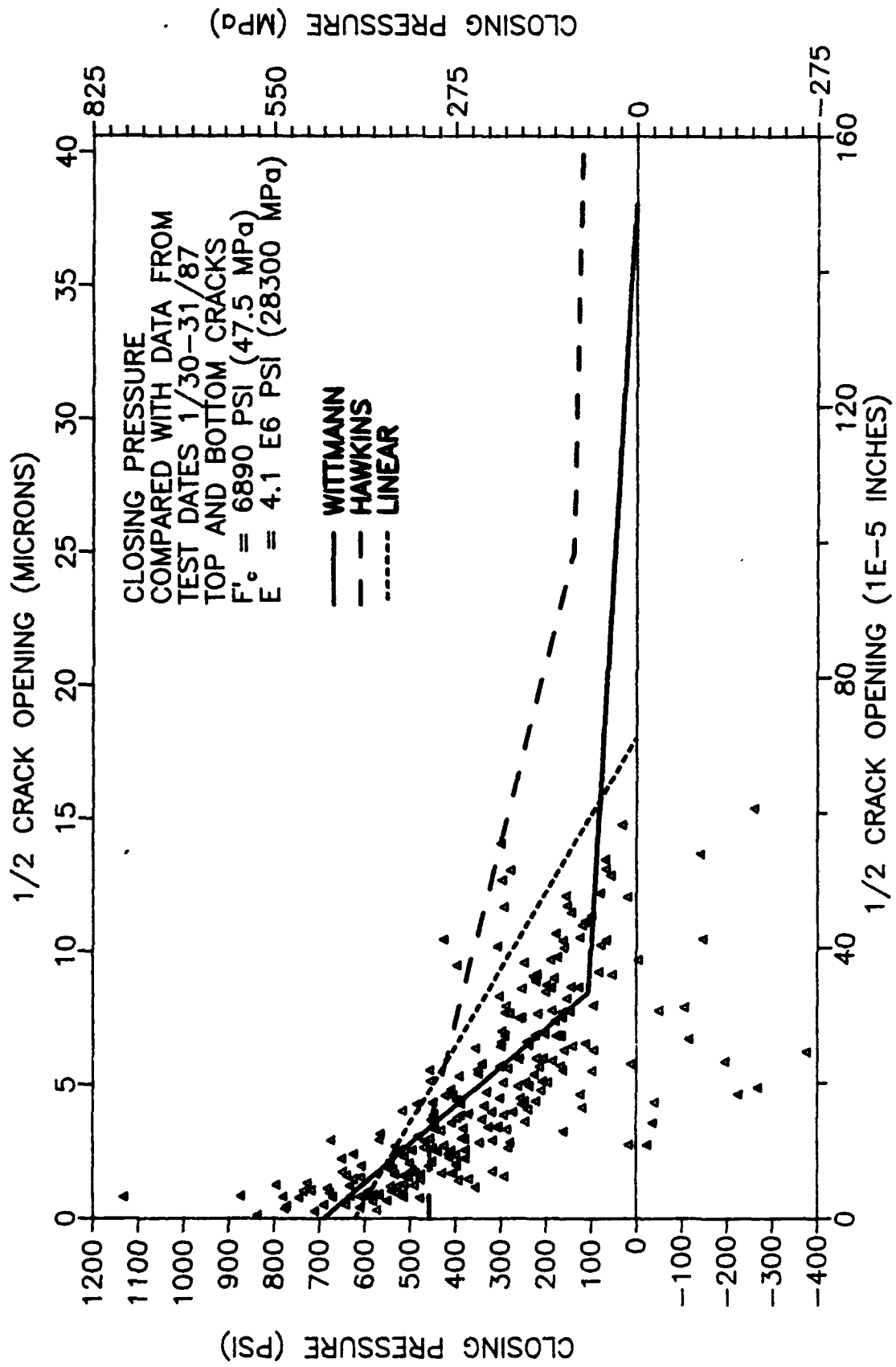


Figure II.10a CLOSING PRESSURE RELATIONSHIPS

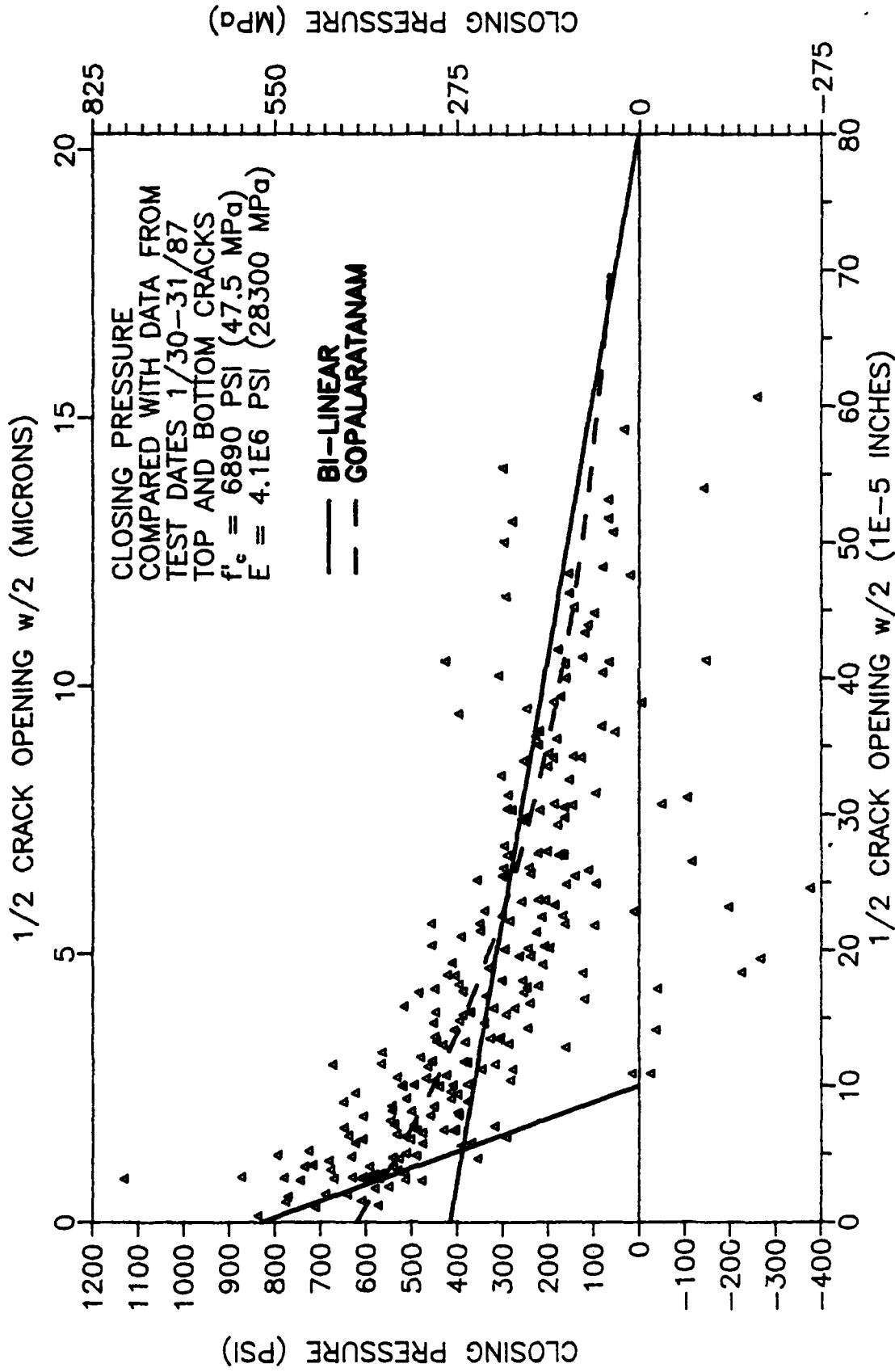


Figure II.10b CLOSING PRESSURE RELATIONSHIPS

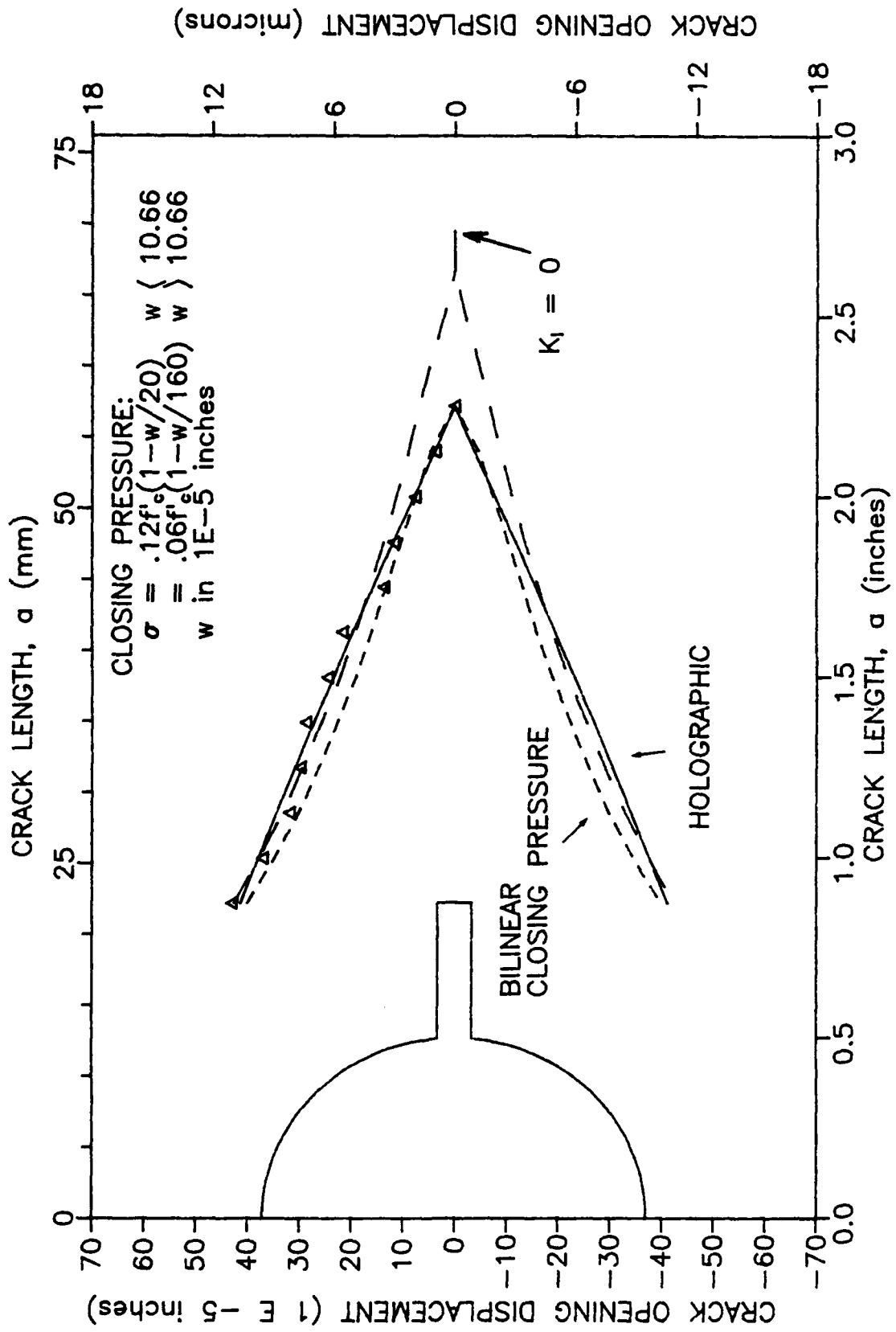


Figure II.11 CRACK PROFILES FOR BILINEAR CLOSING PRESSURE AND DUGDALE MODELS

### PART III: STUDY OF FRACTURE UNDER UNIAXIAL COMPRESSION USING OPTICAL MICROSCOPY

The third phase of the experimental program involved microscopic examination for cracks in concrete cylinders loaded to predetermined levels of axial deformations (uniaxial compression) and then unloaded. Longitudinal and transverse slices were prepared from the unloaded specimens for microscopic examination. The several testing methods to reduce the end-restraint resulting from the specimen-machine effects were studied and the one which gave essentially homogeneous stress distribution was employed in this study.

#### III.1 Mix Proportions and Curing

ASTM Type I cement was used in concrete preparation. The coarse aggregate used was pea gravel of 3/8" nominal size and the fine aggregate was of nominal size 3/16". The specimens were cast in standard 3" x 6" (75 x 150mm) cylindrical cardboard molds and allowed to cure in a curing room for 12 days (approximately 80 percent relative humidity and 75° F). They were taken out, stored in the laboratory while surface was prepared, and were tested at the end of 15 days. The concrete mix proportion used was 1:2.5:2.5:0.6 (cement:sand:aggregate: water by weight).

#### III.2 Petrography

The central test section of each specimen was encased (circumscribed) in a 3.5" (89mm) square epoxy mount. The specimen was placed in a mold made of acrylic plastic and a two-part polyester resin and hardener were cast around the specimen.

The setting time was 10 to 12 hours. The mount was necessary to maintain the integrity of the specimen (especially those loaded to large strains in the strain-softening region) during petrographic preparation.

Specimens loaded to each deformation level were sectioned, one transversely and one longitudinally. 1/2" (12mm) slices were cut from the center of the specimen by sawing with a diamond saw. Slices were washed in a jet of water and allowed to dry in the laboratory for 24 hours. Slices were then stained with pigmented carmine red ink, ground with silicon carbide on rotating laps over a sequence of five grit sizes (180, 240, 320, 400, and 600) and then polished with six-micron diamond paste. The details of the petrographic operations were somewhat similar to those used in Reference 17 and 18 and are described in Reference 19.

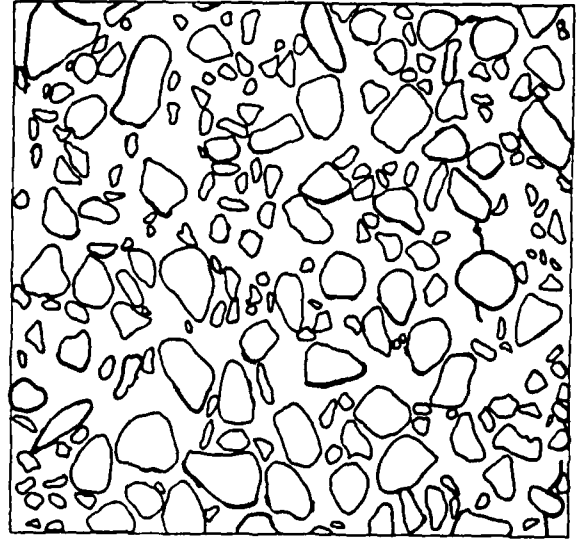
Slices were then examined for microcrack using a stereoscopic microscope (maximum magnification 40x). A microscope lamp which projected light at an angle of 45 illuminated the surface of the specimen. Cracks that were visible as red lines were marked on a photograph of the slice. The average time to mark on one photograph ranged from 10 to 12 hours.

### III.3 Results

For ease of reproduction, cracks were traced from the marked photographs. Some of these tracings are shown in Figures III.1. Observed crack patterns for specimens loaded up to stresses at two values in the ascending part and two values in the descending

part are shown in these figures. From the microscopic study the following key conclusions were drawn:

1. The extent of cracking the prepeak region (stresses less than about 85 percent at peak) is limited primarily to bond cracking (cracks at the interface between the coarse aggregate and mortar matrix) and uniformly distributed in both transverse and longitudinal direction (Figure III.1a), as has also been observed by others (17,18,19).
2. Just prior to peak and immediately after it, major cracking seemed to be localized. This can be observed by examining crack pattern from specimens loaded to about 95 percent of peak stress in the ascending and in the descending regime (Figures III.1a and III.1b). Formation of continuous cracks (mortar and bond cracking) at the two edges of the transverse section can be seen in these figures.
3. Cracking is uniform and extensive over both longitudinal and transverse sections further into the post-peak region (Figure III.1b).
4. The average orientation of mortar-matrix cracks in the longitudinal section was about 80° from the horizontal, indicating that the cracks largely propagated in the loading direction. No shear-band type of failure was observed.
5. As a result of end-restraint, the average stress-strain curve in the strain softening region depends on the gage length as well as the dimensions of the specimen.

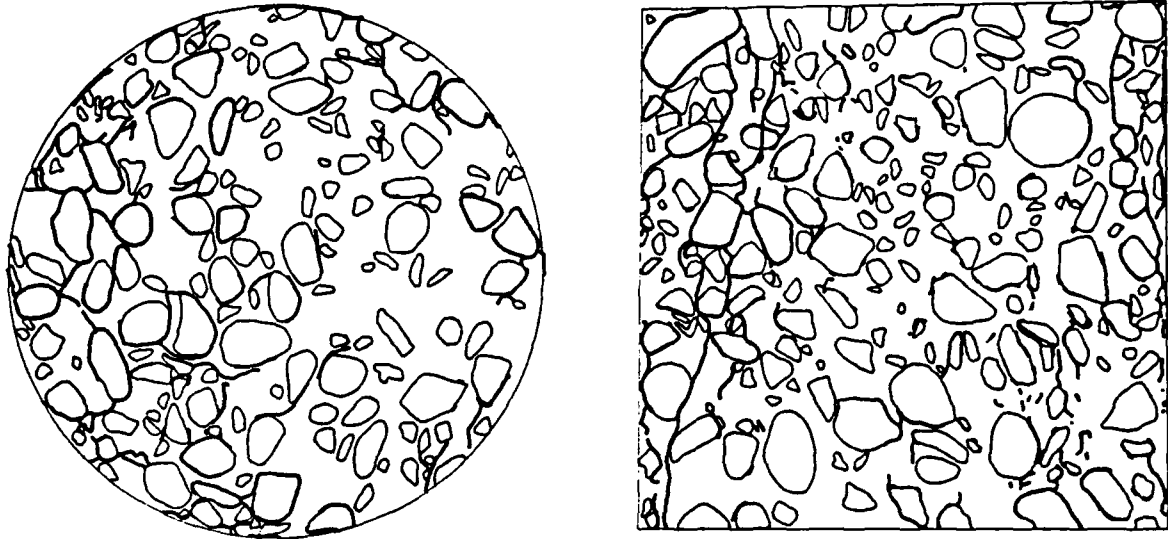


LOAD UP TO  $0.83 f'_c$  IN THE PRE-PEAK REGION

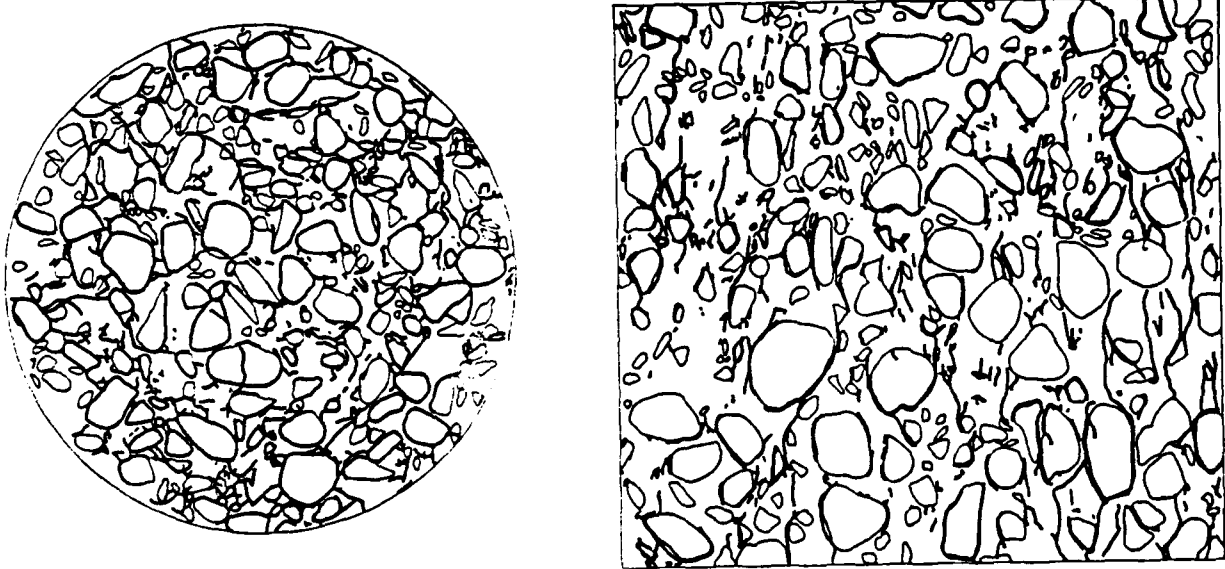


LOAD UP TO PEAK LOAD

Figure III.1a TRACED CRACK PATTERNS FROM CYLINDERS AT DIFFERENT LOAD LEVELS



LOAD UP TO  $0.93 f'_c$  IN THE POST PEAK REGION



LOAD UP TO  $0.81 f'_c$  IN THE POST-PEAK REGION

Figure III.1b TRACED CRACK PATTERN FROM CYLINDERS AT DIFFERENT LOAD LEVELS

PART IV: CRACK PROPAGATION IN UNIAXIAL COMPRESSION:  
HOLOGRAPHIC INTERFEROMETRY

Optical microscopic studies described earlier showed that when concrete specimens are subjected to a uniaxial compression, bond cracks are predominant during the initial stage of loading. To obtain more precise information on how cracks initiate and propagate under compressive loading, "model" concrete specimens were studied using laser holography.

IV.1 Test Specimen

Specimens were 3.75" x 6" x 1" blocks made with mortar with mix proportions by weight of 1:2:.5 (cement, sand, and water respectively). Inclusions were placed as shown in Figure IV.1. The inclusions were limestone aggregates cored out of 12" x 4" x 2" rectangular blocks by a diamond core drill. They were cut to size with a water cooled rotary diamond saw. Plexiglass molds were used to cast the specimens. Specimens were subsequently placed in a curing room for 28 days.

IV.2 Testing Procedure

Specimens were subjected to uniaxial compressive loading in a 120 kip capacity closed-loop testing machine. Axial deformation was used as the feed back. Two LVDTs were mounted on either side of the specimen. LVDTs were attached to aluminum frames which were fixed to a magnetic base.

Real time holograms were made at different stages of loading. The holographic interferometry set-up is shown in Fig. IV.2. The amount of deformation necessary to get a good, well-

spaced fringe pattern was determined from real-time holography. Thereafter, double exposure holograms were made for the same corresponding deformation between the two exposures. Double exposure holograms were preferred because of their increased brightness which made cracks easily visible. The real time holography provided an accurate means of estimating the density of fringes. About 20 double exposure holograms were made during each test at different loading stages. At each stage, the loading platten was held still while holograms were made. The specimen was then loaded to the next stage (slightly higher than the previous one) and held against for the next hologram. Typically observed fringe patterns are shown in Figure IV.3.

#### IV.3 Speckle Photography

This is a simpler method of using monochromatic light from a laser to study displacement of individual points of the object surface (Figure IV.4.). The object surface is illuminated with the expanded and filtered laser light. The object surface thus illuminated contains numerous tiny specks called "speckles" which are caused by diffraction from the irregularities on the object surface. This object surface with speckles is photographed on a typical holographic plate (AGFA 10E75-NAH). The photographic plate would contain the image of the object and the corresponding speckle pattern. The object is then loaded and a second image of the object is made on the same plate (note: the plate is developed only after both the exposures have been completed). The developed plate hence contains two images of the

object and the two corresponding speckle patterns. These two speckle patterns are displaced depending on the displacement of individual points of the object.

If an unexpanded laser beam is now passed through the plate, fringe pattern is observed behind the plate on a screen (Figure IV.5). This is caused by diffraction from the two slightly displaced speckle patterns. The fringe spacing and orientation provide information about the displacement of the point under consideration (the point through which the beam is being passed).

In this experiment, displacements of points on either side of the aggregate matrix interface were measured and the differences were calculated. While  $dH$  denotes the difference in horizontal displacement,  $dV$  denotes the difference in vertical displacement between the two points. Hence,  $dH$  would indicate opening and  $dV$  would indicate sliding (Figures IV.6c and IV.6d).

#### IV.4 Experimental Results

The results of speckle photography are shown in Figure IV.6. Figure IV.6a shows the points (AB & CD) whose displacements were measured. It can be seen from Figure IV.6c that the  $dH/dV$  ratio was close to 1.0 during the initial loading stages, i.e. interface crack was sliding and opening simultaneously. However, close to the peak load, the  $dH/dV$  ratio was much higher, indicating that the crack was mostly opening. Interface cracks therefore originate in mixed mode condition and subsequently become opening mode cracks.

The results of holographic interferometry for specimens containing one inch diameter aggregates are shown in Figure IV.7. The various points at which the holograms were made are shown in the load-deformation diagrams. The cracking pattern observed at six different stages of loading are shown. Bond cracking initiates at loads at about 30% of peak load (Figure IV.7b). The crack patterns correspond to displacement discontinuities which occurred while a small load was applied to the specimen (a little before and after point 1). A crack that disappears on subsequent pictures is a crack that does not open or close. It does not mean that the crack has disappeared or healed. Nonlinearity in the load deformation diagram also starts around that region.

Vertical matrix cracks originate predominantly from these bond cracks and propagate vertically with increased load. Cracks also originate in the matrix under increased loads (Figure IV.7b).

#### IV.5 Summary of Results

1. Cracking initiates at the aggregate-matrix bond leading to nonlinearity in the load-deformation relationship. Bond cracks seem to originate at sites where shear stresses are expected to occur. The measurements of displacement at the interface reveal that bond cracks propagate in the X-Y plane initially in a mixed-mode (both opening and sliding), and subsequently primarily in an opening mode.
2. Bond cracks extend almost all around the aggregate before they extend into mortar matrix. Bond cracks initiate in the

shear mode. Angularity and frictional resistance of the aggregate are thus more relevant at this loading stage (30% to 80% of peak load) after bond crack begins and before matrix cracks dominate.

3. Matrix cracks originate predominantly at the interface and propagate in the direction of the applied load. These cracks originate from near the top and bottom of the aggregate and propagate almost vertically. No gradual curvature from inclined bond crack to vertical matrix crack was generally observed. Matrix cracks from voids also propagate in the same manner but at the top or bottom of the holes. It appears that the initiation and growth of matrix cracking is dominated by the mode 1 stress intensity factor. Matrix cracking from the holes originates near the top and bottom, further substantiating this view.

4. Diagonal cracking joins the otherwise vertical mortar cracks close to peak load. This leads to a continuous crack across the length of the specimen. These diagonal cracks are probably a result of end-constraint and may also be caused by the interaction of X-Z plane by tensile cracks in the Y-Z plane.

5. Failure occurs when sufficient tensile cracking has occurred to cause local buckling and general instability in the specimen. Localized cracking and consequent instability may therefore explain concrete behavior in compression.

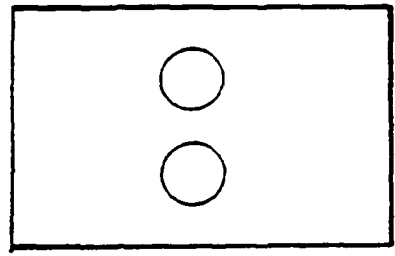
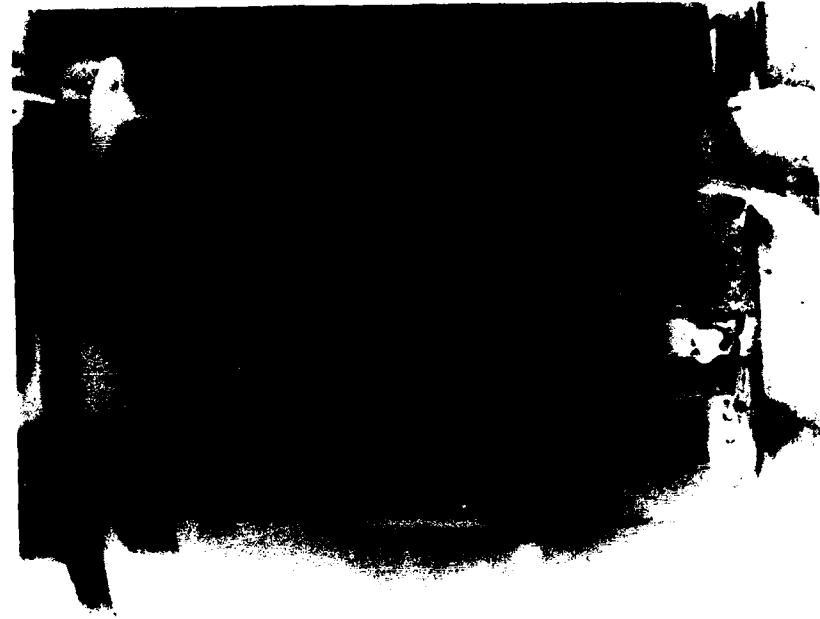
6. Nonlinearity in concrete is a function of the size of aggregates and voids. Mortar and voids exhibit less nonlinear behavior than specimens with aggregates of the same diameter as

that of the void.

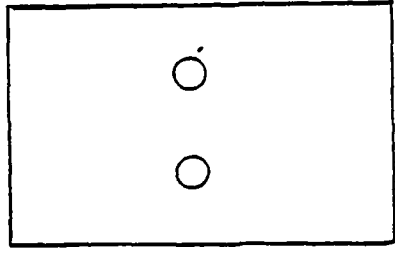
7. Less interfacial cracking was observed in specimens with smaller aggregates.

8. Conclusions 6 and 7 are based on observations that specimens with a 1" aggregate showed more bond cracking and exhibited a more nonlinear load-displacement than those with 1/2" aggregates. In contrast, specimens with 1" holes showed less matrix cracking and less nonlinear response than those with 1/2" holes. Thus the aggregate dimension and void dimension have differing effects on the overall response of concrete.

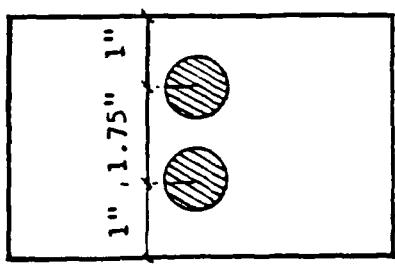
9. A combination of acoustic and optical techniques employed in a closed loop test set-up can be further adopted to different specimen geometry and loading configurations.



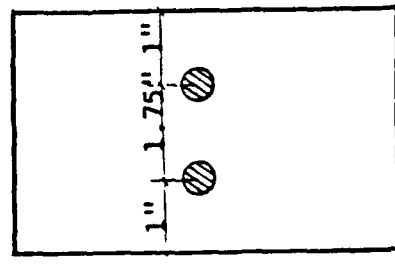
1" VOID



1/2" VOID

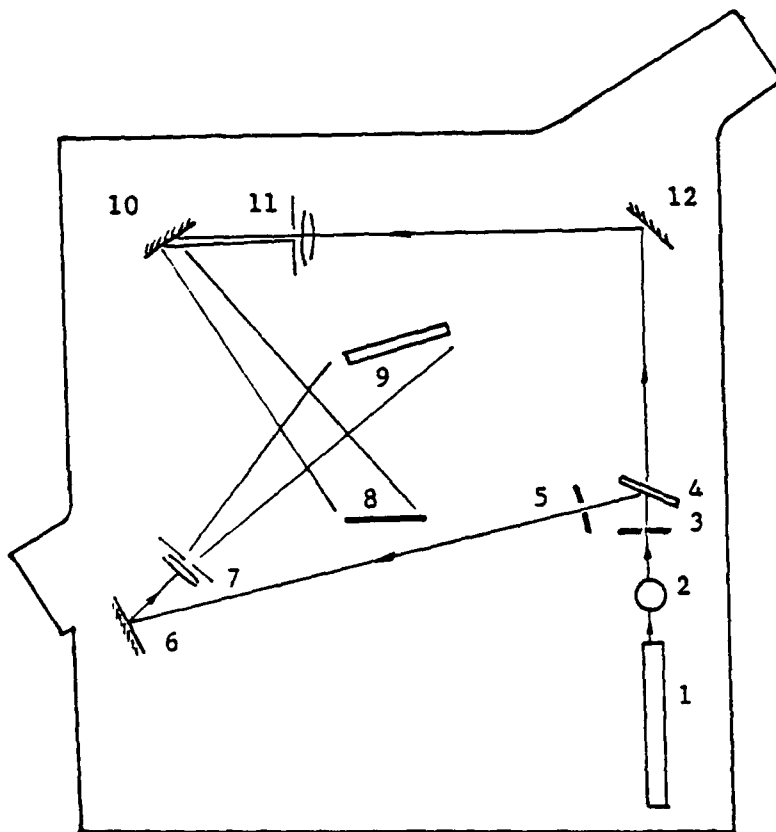


1" AGGREGATE



1/2" AGGREGATE

Figure IV.1 EXPERIMENTAL SET-UP FOR COMPRESSION TEST



## INDEX

1. LASER
2. BEAM STEERING MIRROR
3. SHUTTER
4. BEAM-SPLITTER
5. SHUTTER
6. MIRROR
7. SPATIAL FILTER
8. HOLOGRAPHIC FILM
9. SPECIMEN
10. REFERENCE MIRROR
11. SPATIAL FILTER
12. MIRROR

Figure IV.2 HOLOGRAPHIC INTERFEROMETRY SET-UP

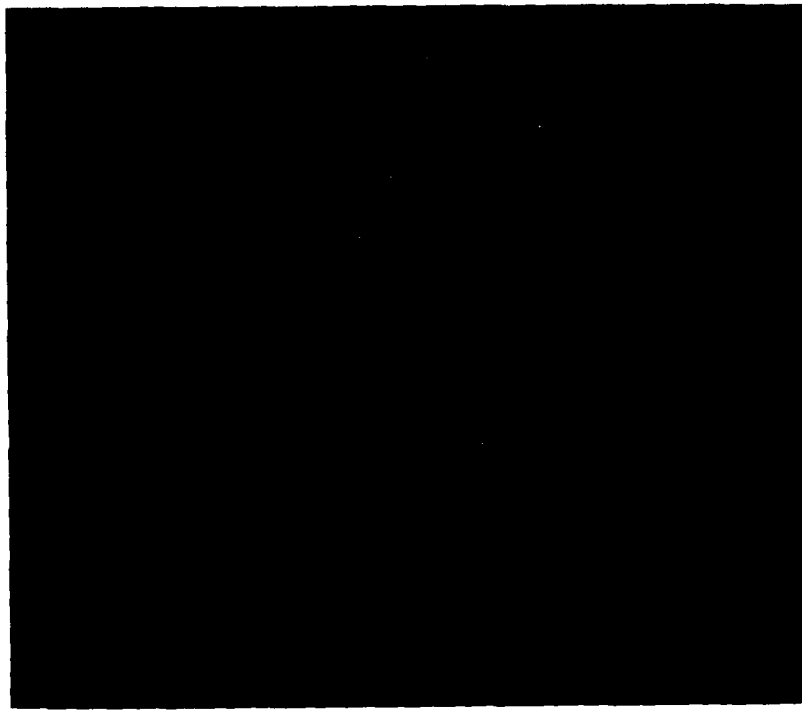
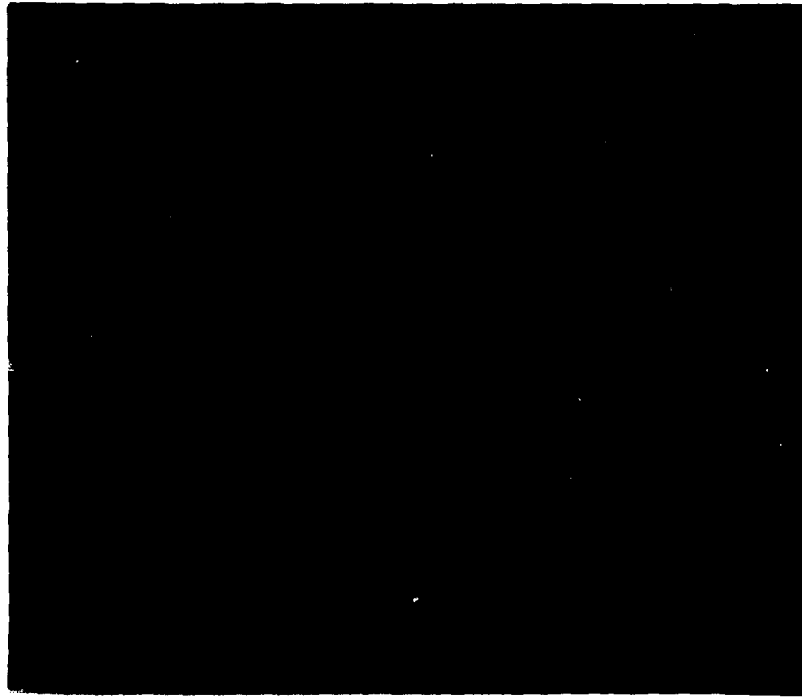


Figure IV.3 CRACK PATTERNS FROM HOLOGRAPHIC INTERFEROMETRY

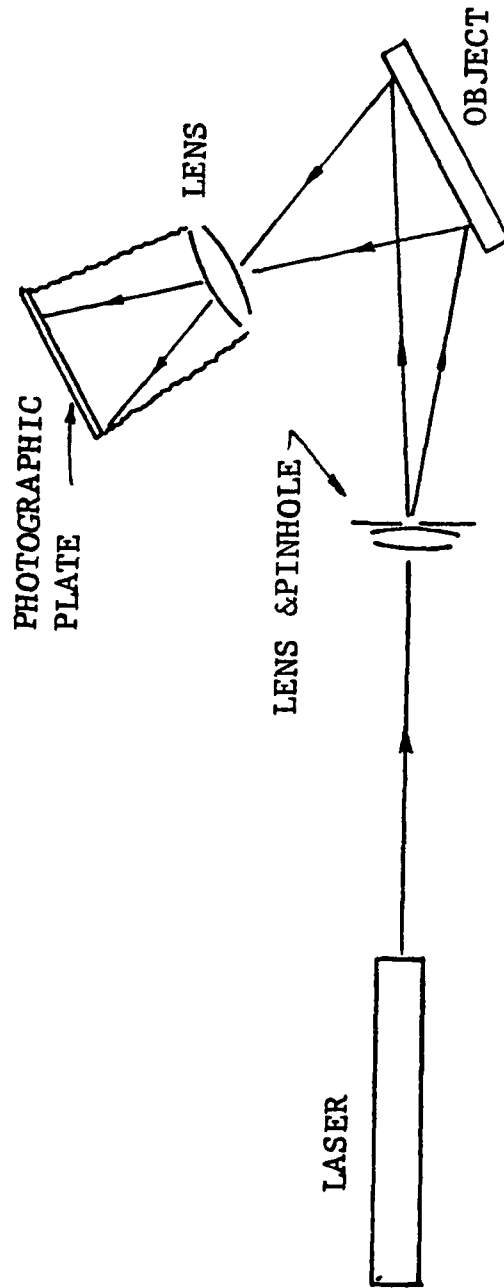


Figure IV.4 LAYOUT FOR SPECKLE PHOTOGRAPHY

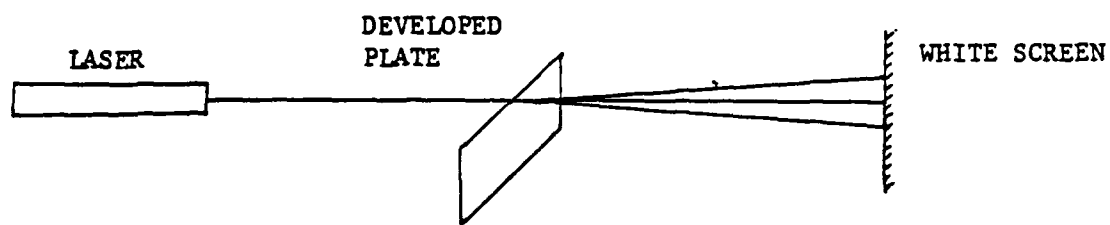


Figure IV.5a SET-UP FOR INTERPRETING SPECKLE PHOTOGRAPHS

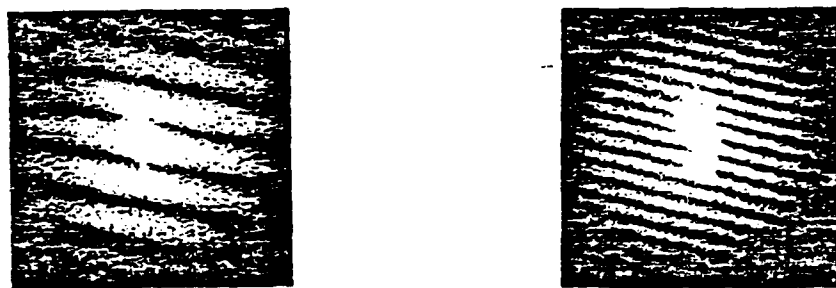


Figure IV.5b TYPICAL FRINGES FROM SPECKLE PHOTOGRAPHS

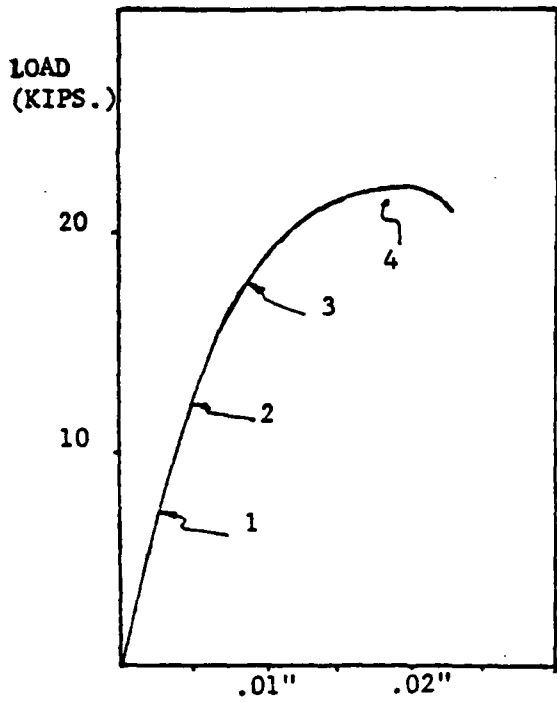


Figure IV.6a LOAD DISPLACEMENT DIAGRAM FOR SPECKLE PHOTOGRAPHY

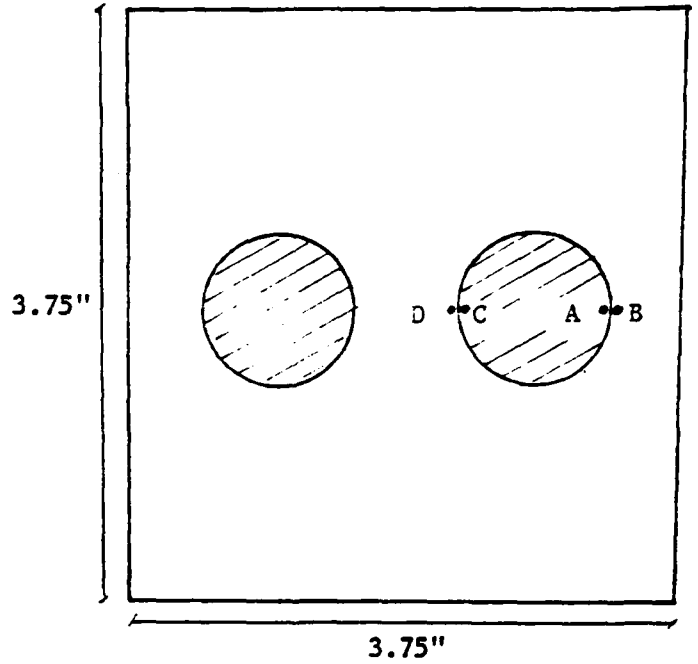


Figure IV.6b POINTS OF THE SPECIMEN TESTED FOR DISPLACEMENT

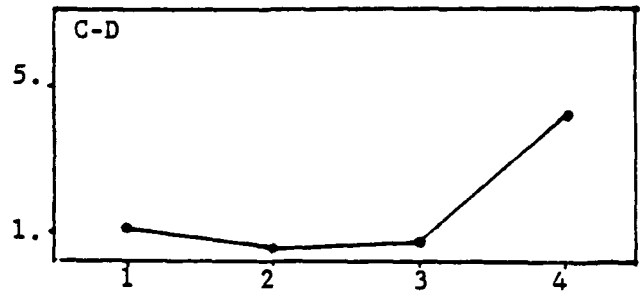
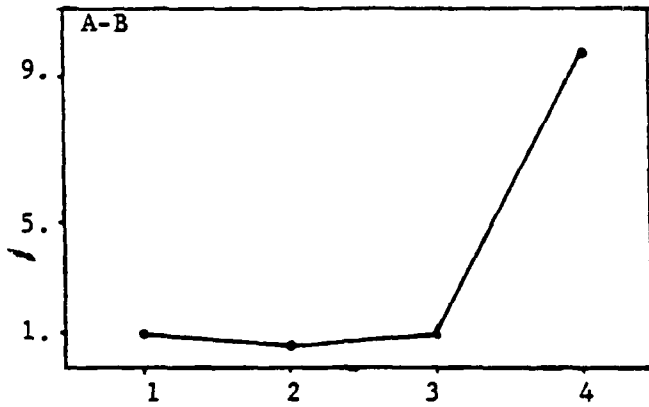


Figure IV.6c & d dh/dv RATIO FOR POINTS A-B, C-D DURING LOADING STAGES 1-4

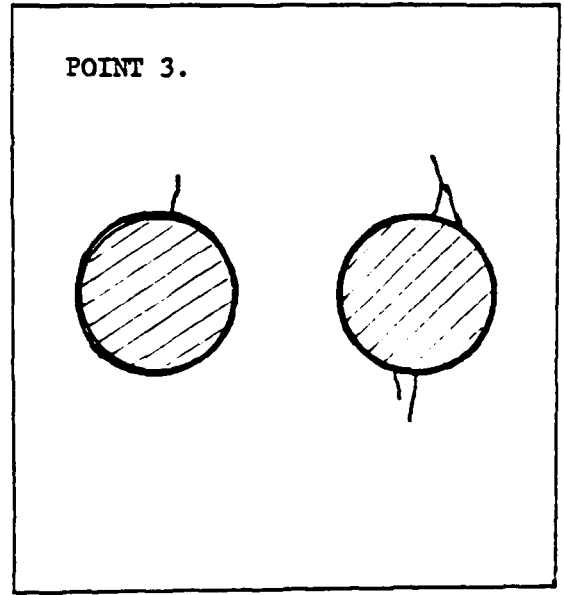
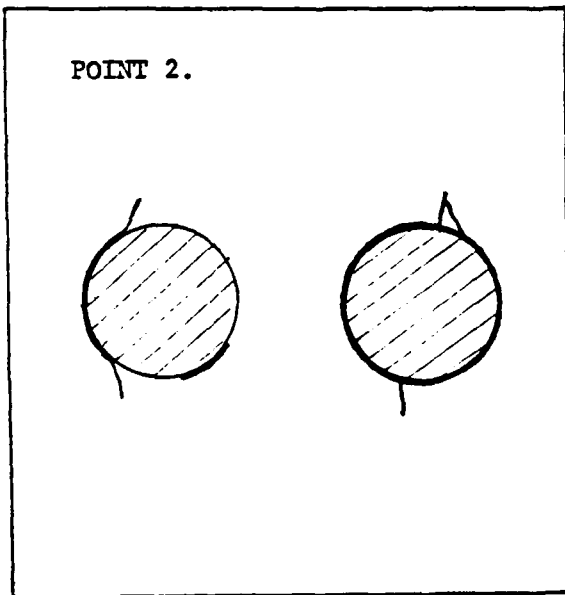
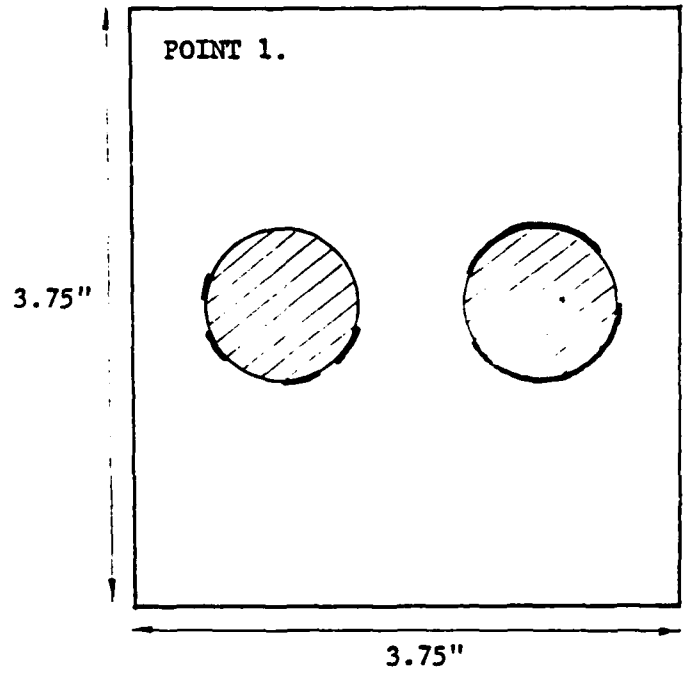
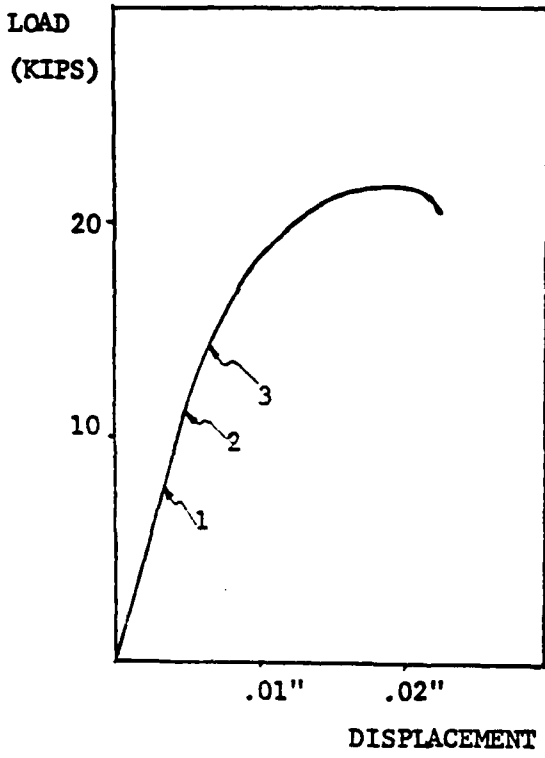


Figure IV.7a LOAD-DISPLACEMENT CURVE AND CRACK PATTERN FOR  
1" AGGREGATE SPECIMEN

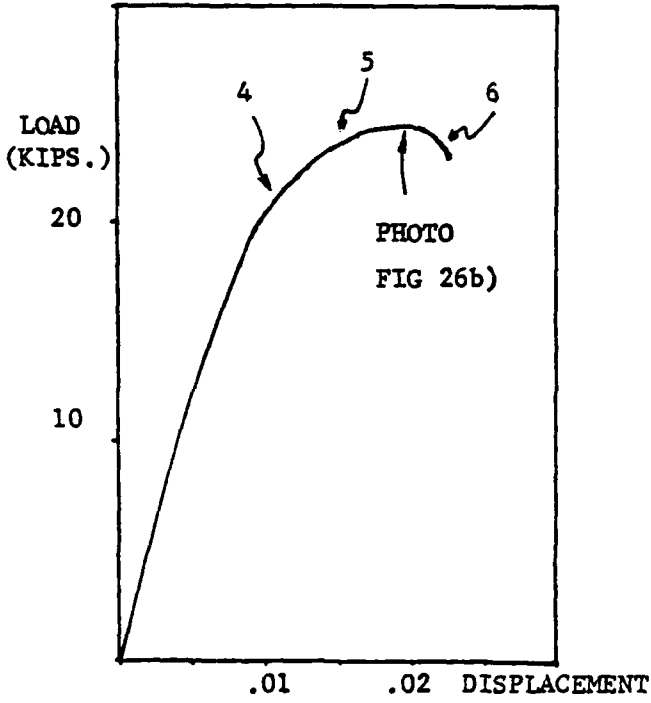


FIGURE 13a LOAD-DISPLACEMENT DIAGRAM FOR HOLOGRAPHIC INTERFEROMETRY TEST

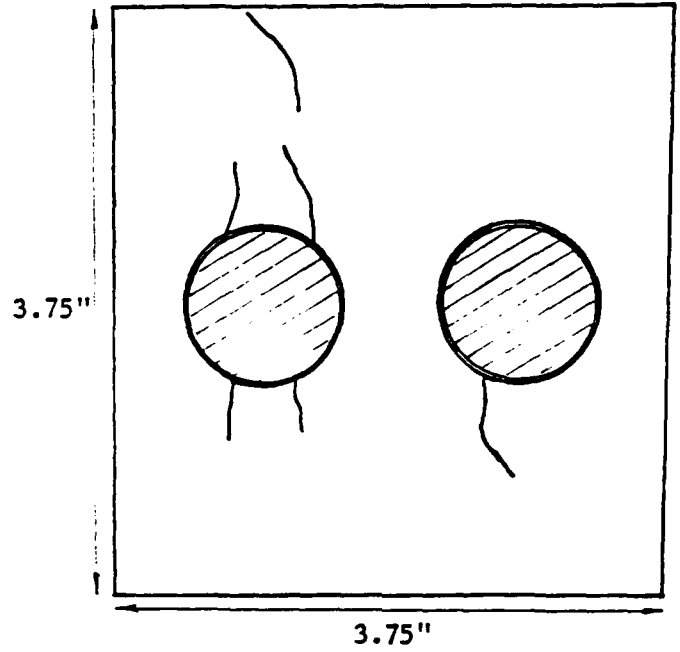


FIGURE 13b. CRACK PATTERN AT POINT 4.

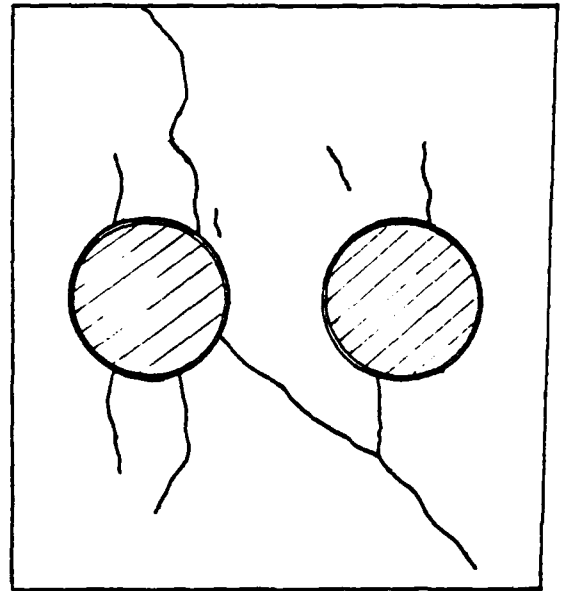
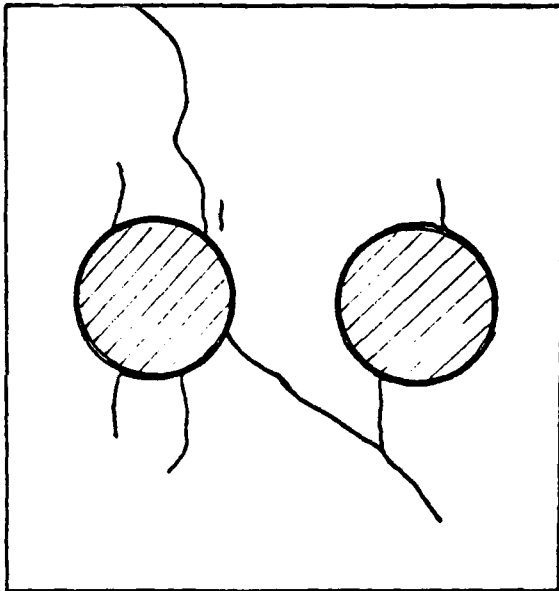


Figure IV.7b LOAD-DISPLACEMENT CURVE AND CRACK PATTERN FOR 1" AGGREGATE SPECIMEN

## REFERENCES

1. Hamstad, M.A., "A Review: Acoustic Emission, A Tool for Composite Materials Studies," *Experimental Mechanics*, March 1986.
2. Izsumi, M., Mihashi, H., and Nomura, N. "Acoustic Emission Technique to Evaluate Fracture Mechanics Parameter in Concrete," *Proceedings of the Seventh International Acoustic Emission Symposium*, 200, Japan, October 23-26, 1984
3. Tanigawa, Y., Yamada, K., Kiriya, S. "Frequency Characteristics of Acoustic Emission Waves in Concrete," *Transactions of the Japan Concrete Institute*, Vol. 2, pp. 155-162, 1980.
4. Labusz, J., Shah, S.P., and Dowding, C.H., "Measurements and Description of the Tensile Fracture Process of Rock," *Int. J. of Rock Mechanics and Mining Sciences*, 24(4), August 1987, pp. 235-246.
5. Scruby, C.B., Baldwin, G.R., Stacey, K.A., "Characterization of Fatigue Crack Extension by Quantitative Acoustic Emission," *International Journal of Fracture* 28, 201-222, 1985.
6. Michaels, J.E., Michaels, T.E., and Sachse, W., "Applications of Deconvolution to Acoustic Emission Signal Analysis," *Materials Evaluation*, 1391, p. 1032, 1981.
7. Gopalaratnam, V.S. and Shah, S.P., "Softening Response of Plain Concrete in Direct Tension," *ACI Journal*, 310-323, May-June 1985.
8. Bazant, Z.P. and Oh, B.H., "Crack Band Theory for Fracture of Concrete," *Materials and Structures*, Vol. 16, No. 93, May-June 1983, pp. 155-177.
9. Hillerborg, A., Modeer, M. and Peterson, P.E., "Analysis of Crack Formation and Crack Growth in Concrete by Means of Fracture Mechanics and Finite Elements," *Cement and Concrete Research*, Vol. 6, No. 6, November, 1976, pp. 773-782.
10. Jenq, Y.S. and Shah, S.P., "A Fracture Toughness Criterion for Concrete," *Engineering Mechanics*, Vol. 21, No. 5, 1985, pp. 1055-1069.

11. Kobayashi, A.S., Hawkins, N.M., Barker, D.B. and Liaw, B.M., "Fracture Process Zone of Concrete," Proceedings of NATO Advanced Workshop on Application of Fracture to Cementitious Composites, S.P. Shah, Ed., NATO-ARW, Northwestern University, 1984.
12. Wacharatana, M. and Shah, S.P., "Prediction of Non-Linear Fracture Process Zone in Concrete," Journal of Engineering Mechanics Division, ASCE, June 1983, pp. 1100-1113.
13. Abramson, N., The Making and Evaluation of Holograms, Academic Press, 1981.
14. Abramson, N. and Bjelkhagen, H., "Sandwich Hologram Interferometry. (Part) 5. Measurement of In-plane Displacement and Compensation for Rigid Body Motion," Applied Optics, Vol. 18, No. 16, 1979, p. 2890.
15. Nelson, D.V. and McCrickerd, J.T., "Residual Stress Determination Through Combined Use of Holographic Interferometry and Blind Hole Drilling," Experimental Mechanics, Vol. 26, No. 4, Dec. 1986, pp. 379-385.
16. Jenq, Y.S. and Shah, S.P. "Two Parameter Model for Concrete," Journal of Engineering Mechanics, ASCE, Vol. 111, No. 10, Oct. 1985, pp. 1227-1241.
17. Hsu, Thomas, T.C., Slate, Floyd O., Sturman, G.M., and Winter, G., "Microcracking of Plain Concrete and Shape of the Stress-Strain Curve," ACI Journal, Proceedings, Vol. 60, No. 2, Feb. 1963, pp. 209-224.
18. Shah, S.P. and Winter, G., "Inelastic Behavior and Fracture of Concrete," ACI Journal, Proceedings Vol. 63, No9, Sept. 1966, pp. 925-930.
19. Shah, S.P. and Chandra, S., "Critical Stress, Volume Change, and Microcracking of Concrete," ACI Journal, Proceedings Vol. 65, No. 9, Sept. 1968, pp. 770-781.